frontiers | Frontiers in Nanotechnology

TYPE Original Research
PUBLISHED 25 August 2025
DOI 10.3389/fnano.2025.1587084

Check for updates

OPEN ACCESS

EDITED BY
Majid Jabir,
University of Technology, Iraq

REVIEWED BY
Ashish Kapoor,
Harcourt Butler Technical University, India
Bilal Ahmed,
Khwaja Fareed University of Engineering and Information Technology (KFUEIT), Pakistan

*CORRESPONDENCE
Hajer S. Alorfi,
halorfi@kau.edu.sa
Amna N. Khan,
ankmohamad@kau.edu.sa

†These authors have contributed equally to this work

RECEIVED 08 March 2025
ACCEPTED 28 July 2025
PUBLISHED 25 August 2025

CITATION
Alorfi HS, Alomari MS, Bawakid NO, Althagbi HI, Alsebaii NM, Aslam M, Chandrasekaran S, Soomro MT and Khan AN (2025) Green synthesis of AgNPs using *Forsskaolea tenacissima*: sustainable nanotechnology for antimicrobial, antioxidant, and catalytic activities.
Front. Nanotechnol. 7:1587084.
doi: 10.3389/fnano.2025.1587084

COPYRIGHT
© 2025 Alorfi, Alomari, Bawakid, Althagbi, Alsebaii, Aslam, Chandrasekaran, Soomro and Khan. This is an open-access article distributed under the terms of the Creative Commons Attribution License (CC BY). The use, distribution or reproduction in other forums is permitted, provided the original author(s) and the copyright owner(s) are credited and that the original publication in this journal is cited, in accordance with accepted academic practice. No use, distribution or reproduction is permitted which does not comply with these terms.

Green synthesis of AgNPs using *Forsskaolea tenacissima*: sustainable nanotechnology for antimicrobial, antioxidant, and catalytic activities

Hajer S. Alorfi[1*†], Maha S. Alomari[1†], Nahed O. Bawakid[1], Hanan I. Althagbi[2], Naha M. Alsebaii[1], M. Aslam[3], S. Chandrasekaran[3], M. Tahir Soomro[3] and Amna N. Khan[1*]

[1]Department Chemistry, Faculty of Science, King Abdulaziz University, Jeddah, Saudi Arabia, [2]Department of Chemistry, College of Science, University of Jeddah, Jeddah, Saudi Arabia, [3]Center of Excellence in Environmental Studies, King Abdulaziz University, Jeddah, Saudi Arabia

Antimicrobial resistance is rapidly increasing worldwide, leading to higher mortality rates, particularly among children, as improper antibiotic use renders treatments less effective. Plant-derived AgNPs have emerged as sustainable natural agents, offering enhanced antimicrobial activity against multidrug-resistant bacteria without promoting further resistance. In this context, the *Urticaceae* plant *Forsskaolea Tenacissima* (*F. Tenacissima*), with its rich phytochemical content and traditional medicinal uses, remains largely unexplored for green AgNP synthesis. Motivated by this gap, we investigated *Ft*-AgNPs as a novel antimicrobial, antioxidant, and catalytic agent. Compared to well-studied plants like *Azadirachta indica* and *Ocimum sanctum*, *F. Tenacissima* offers a distinct and potentially more potent phytochemical composition, making it a promising candidate for sustainable AgNPs synthesis. The synthesis was rapid and efficient, with the *F. Tenacissima* aqueous leaf extract serving as both reducing and stabilizing agent in the formation of *Ft*-AgNPs. UV-Visible spectroscopy revealed a characteristics absorption peak at 446 nm, confirming the formation of *Ft*-AgNPs. SEM analysis showed densely packed, spherical *Ft*-AgNPs, while a zeta potential of −28.1 mV indicated strong electrostatic repulsion, suggesting good colloidal stability. DLS analysis supported the size distribution observed in TEM images, and XRD confirmed the crystalline nature and face-centered cubic (fcc) structure of *Ft*-AgNPs. FTIR and HPLC analysis identified 4-hydroxybenzoic acid and salicylic acid in the plant extract, which played a key role in the reduction of Ag^+ ions and stabilization of *Ft*-AgNPs. The antibacterial efficacy of *Ft*-AgNPs was demonstrated against *B. cereus, E. coli*, and *P. aeruginosa* using disk diffusion and serial dilution methods. For antifungal activity, two yeasts species, *C. albicans* and *C. glabrata*, were tested. Antioxidant potential was assessed through the DPPH radical scavenging assay, while catalytic activity was evaluated via the reduction of two common wastewater pollutants, 4-nitrophenol (4-NP) and methylene blue (MB), using *Ft*-AgNPs and $NaBH_4$. Overall, the study highlights the efficient

green synthesis of *Ft*-AgNPs with remarkable antimicrobial, antioxidant, and catalytic properties, offering a sustainable and effective approach for the development of multifunctional nanomaterials.

KEYWORDS

Forsskaolea tenacissima, aqueous leaf extract, green synthesis, silver nanoparticles, sustainable approach, antimicrobial activity, antioxidant and catalytic properties

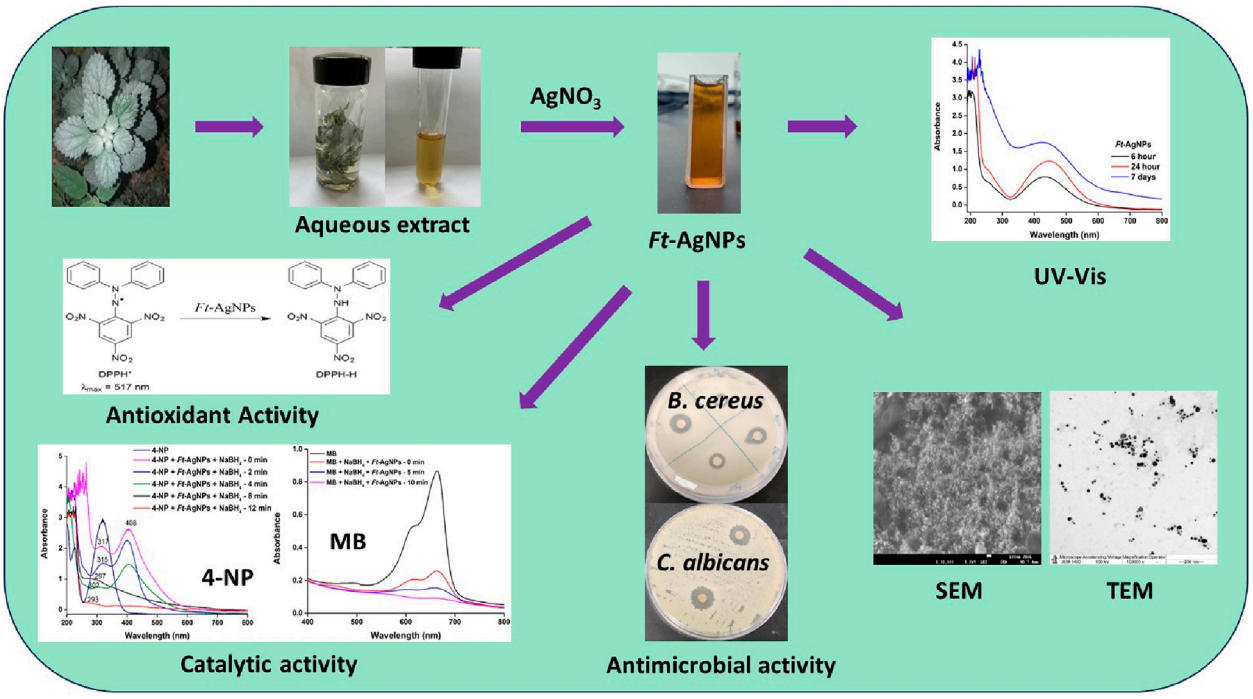

GRAPHICAL ABSTRACT

1 Introduction

With the advent of antibiotics, many were originally isolated from natural sources and later chemically synthesized. However, the overuse and indiscriminate application of these drugs have led to a significant rise in bacterial resistance (Bérdy, 2012; Frère and Rigali, 2016). Consequently, human health is increasingly threatened by the resurgence and spread of various bacterial diseases (Aljamali et al., 2021). To overcome this growing challenge, researchers have turned to the engineering of NPs from natural sources as a promising alternative (Moloney, 2016). Plant-derived NPs exhibited multiple mechanisms of antimicrobial action, including disruption of bacterial membranes, release of ions, generation of reactive oxygen species (ROS), and binding to bacterial DNA (Hernández-Díaz et al., 2021). Additionally, their surfaces are enriched with bioactive compounds such as flavonoids, polyphenols, and phenolic acids, which contributed to synergistic antimicrobial effects and made it significantly more difficult for bacteria to develop resistance (Anand et al., 2022).

Recent studies have reported that more than 70% of bacterial strains are resistant to one or more antibiotics, often forcing physicians to increase antibiotic dosages, which in turn raises the risk of adverse reactions (Nwobodo et al., 2022). Furthermore, some severe bacterial infections have become increasingly difficult, or even impossible to cure (Uyttebroek et al., 2022). These alarming trends have driven the search for new antibacterial strategies, including the development of novel therapeutics from natural products and the modification of existing antibiotic classes (Moloney, 2016). As a result, NPs, particularly AgNPs have emerged as a highly effective option for treating various infections, especially those caused by multidrug-resistant (MDR) bacteria and fungi (Mateo and Jiménez, 2022; More et al., 2023). The surface engineering of plant-derived AgNPs plays a crucial role in enhancing their antimicrobial efficacy by promoting strong interactions with bacterial cells, facilitating their internalization, releasing Ag^{+} ions, and simultaneously targeting multiple intracellular components (Khan et al., 2022). This multi-faceted mechanism leads to the generation of high oxidative stress within bacterial cells, effectively reducing bacterial resistance and slowing the spread of infection.

Considering their clinical significance and relevance to real-world applications, we selected a diverse panel of bacterial and fungal strains in this study to represent a broad spectrum of pathogens. *B. cereus* (Gram-positive) is commonly associated with foodborne illness, particularly from improperly stored or undercooked food (Jaha et al., 2016). *E. coli* (Gram-negative), a facultative anaerobe found in the intestines of warm-blooded animals, includes pathogenic

strains responsible for serious infections (Jaha et al., 2016). *P. aeruginosa* (Gram-negative) is a major cause of hospital-acquired infections such as pneumonia and urinary tract infections (Jaha et al., 2016). *C. albicans* is a leading cause of superficial fungal infections like oral thrush and vaginal candidiasis (Katsipoulaki et al., 2024). *C. glabrata*, increasingly linked to candidemia, is a growing concern in the healthcare sector due to its reduced susceptibility to antifungal treatments (Katsipoulaki et al., 2024). Thus, the selected bacterial and fungal strains represent a mix of Gram-positive and Gram-negative bacteria, as well as drug-susceptible and drug-resistant fungi, all of which are relevant in clinical and environmental contexts. Evaluating the antimicrobial activity of *Ft*-AgNPs against this diverse panel helps demonstrate their broad-spectrum potential and real-world applicability in addressing public health challenges related to microbial resistance, contamination, and infection control.

ROS include free radicals like superoxide anion and hydroxyl radicals, along with non-radical species such as hydrogen peroxide and singlet oxygen. An active antioxidant defense system is crucial for maintaining a balance in free radical production (Martemucci et al., 2022). Deficiencies in this system can contribute to chronic diseases, including diabetes, cancer, atherosclerosis, arthritis, neurodegenerative disorder, and accelerated aging (Sadiq, 2023). While AgNPs induce bacterial cell death through ROS generation withing the cell, they can also offer protection to the human body (Thanh et al., 2022). Plant-derived AgNPs efficiently scavenge ROS through two mechanisms, providing electron donation and hydrogen release via surface-functionalized groups, thereby preventing oxidative stress and damage caused by free radicals (Palithya et al., 2021). Additionally, over the past 2 decades, AgNPs have been widely studied as catalysts in environmental remediation, effectively removing pollutants like nitrophenols and textile dyes, often in combination with $NaBH_4$ (Fatiqin et al., 2024; Charti et al., 2021). Some studies even regard AgNPs as the gold standard for removing nitrophenols from wastewater. Consequently, the application of plant-derived AgNPs in pollutant removal has surged.

Traditionally, AgNPs have been synthesized using various physical and chemical methods, which, while effective, have several drawbacks, including high costs, significant energy consumption, and the use of toxic substances (Nie et al., 2023). In contrast, the synthesis of AgNPs using natural sources, such as plant extracts, is more environmentally friendly, cost-effective, and less toxic (Kulkarni et al., 2021). Plant extracts naturally contain both reducing and stabilizing agents that facilitate rapid AgNPs formation. Beyond plant extracts, the use of other natural bioactive agents such as microbes, biowastes (e.g., vegetable and fruit peel waste, eggshells, agricultural byproducts) and algae has also been explored as sustainable alternatives to avoid the production of undesirable or hazardous byproducts (Kaur, 2024). Green synthesis of AgNPs offers numerous advantages, including simplicity, cost-effectiveness, high nanoparticle stability, minimal time requirements, the generation of non-toxic byproducts, and ease of scaling up for larger-scale production (Alharbi et al., 2022; Kaabipour and Hemmati, 2021). Among natural sources, plant-derived AgNPs are more prominently reported in literature, primarily due to the ease of handling plant materials at room temperature compared to maintaining microbial cultures, algae, or other biological systems (Pate et al., 2023). Typically, AgNPs can be synthesized simply by mixing an aqueous plant extract with a metal precursor solution at ambient conditions. However, several factors including the type of plant, aqueous or non-aqueous extracts, concentration of bioactive compounds, pH, temperature, and the contact time with the metal precursor play critical roles in controlling the size, shape, aggregation behavior, surface functionalization, and ultimately, the properties of the resulting AgNPs (Azad et al., 2023).

Botanical families such as *Urticaceae* and *Bignoniaceae* include plants of significant medicinal and biological importance. The *Urticaceae* family comprises approximately 2,000 species across 54 genera, predominantly found in tropical regions (Assaf et al., 2021). Among these, the genus *Forsskaolea* is particularly notable, with a distribution spanning the Canary Islands, southeastern Spain, India, Pakistan, Egypt, and southwestern Saudi Arabia (Assaf et al., 2018; Assaf et al., 2015). *F. tenacissima* is a member of this genus and is classified as a non-stinging nettle. Extracts of *F. tenacissima* have demonstrated notable therapeutic potential, suggesting a rich and diverse chemical composition with numerous bioactive compounds (Assaf et al., 2015; Sher et al., 2017; Roy et al., 2017; Singhal et al., 2011; Kirthika et al., 2025; Subramani et al., 2024). Several studies have reported its antibacterial antiviral, antioxidant, and antipyretic activities, along with applications in diabetes management, atherosclerosis reversal, and liver protection (Assaf et al., 2015; Sher et al., 2017; Roy et al., 2017; Singhal et al., 2011; Kirthika et al., 2025; Subramani et al., 2024). Phytochemical investigations have revealed that *F. tenacissima* is rich in triterpenese, flavonoids, sterols, polyphenols, and phenolic acids, compounds highly valued for various biological and industrial applications, including nanoparticles synthesis (Assaf et al., 2018; Assaf et al., 2015; Sher et al., 2017; Roy et al., 2017; Singhal et al., 2011; Kirthika et al., 2025; Subramani et al., 2024). However, to the best of my knowledge, the synthesis of AgNPs using *F. tenacissima* extracts has not been previously reported. Thus, utilizing the aqueous leaf extract of *F. tenacissima* for AgNPs synthesis presents a novel and promising strategy.

Herein, the aqueous leaf extract of *F. tenacissima* was prepared and utilized for the green synthesis of AgNPs. The resulting nanoparticles were labeled as *Ft*-AgNPs for simplicity and were thoroughly characterized using UV-Visible, FTIR, HPLC, XRD, SEM, TEM, DLS, and Zeta potential analysis. The bioactive compounds present in the aqueous extract were identified, and a simplified mechanism for the synthesis of *Ft*-AgNPs was proposed. The antibacterial and antifungal activities of *Ft*-AgNPs were evaluated against three bacterial strains (*B. cereus, E. coli*, and *P. aeruginosa*) and two fungal strains (*C. alibicans* and *C. glabrata*), with the antimicrobial mechanism discussed in brief. The antioxidant potential of *Ft*-AgNPs was assessed through DPPH radical scavenging assay, while their catalytic efficiency was demonstrated through the reduction of 4-NP and MB.

2 Experimental

2.1 Chemical and reagents

The chemicals utilized in this study included silver nitrate ($AgNO_3$), sodium hydroxide (NaOH), ethanol, ascorbic acid, DPPH radical, 4-nitrophenol, methylene blue, were of high purity, purchased from Sigma-Aldrich, and used without further

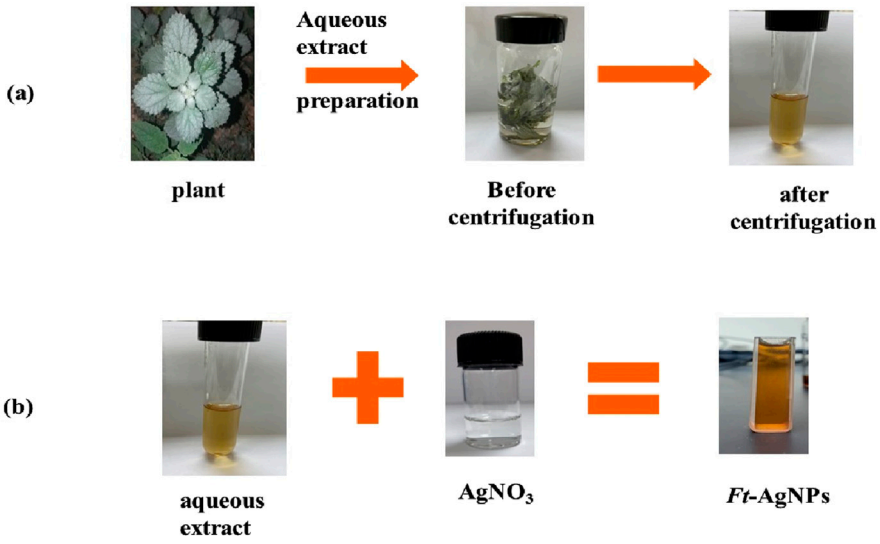

SCHEME 1
Simplified steps for the preparation of **(a)** aqueous extract of *F. tenacissima* leaves and **(b)** synthesis of *Ft*-AgNPs.

purification. All solutions and media were prepared using double distilled water. Fresh leaves of *F. tenacissima* were collected from Al-Baha, Saudi Arabia and identified based on plant taxonomy and literature survey. The leaves were thoroughly washed with double distilled water to remove dust and adhering particles, air-dried at room temperature, and subsequently stored in sealed plastic bags until further use.

2.2 Aqueous extract preparation and *Ft*-AgNPs synthesis

To maximize the extraction of bioactive compounds, 0.5 g of dried leaves of *F. tenacissima* were soaked in 10 mL of double-distilled water and kept at room temperature for 24 h. This process resulted in an aqueous *F. tenacissima* extract with a concentration of 50 mg/mL, providing a rich source of phytochemicals that serve as natural reducing and capping agents for *Ft*-AgNPs synthesis. The mixture was then centrifuged at 5,000 rpm for 5–10 min to remove any residual insoluble biomass. The resulting clear, light brown extract was collected and stored at 4°C until further use.

The aqueous *F. tenacissima* extract was subsequently diluted to an effective concentration range of 1,000 µg/mL during the synthesis process to ensure that sufficient phytochemical content was present in the reaction mixture for the effective reduction of Ag^+ ions and stabilization of the resulting AgNPs, leading to the formation of *Ft*-AgNPs. In brief, 100 µL of 0.1 M $AgNO_3$ solution (containing 10.787 mg/mL of Ag^+) was mixed with 100 µL of the 50 mg/mL aqueous *F. tenacissima* extract in 5 mL of distilled water. This resulted in final concentrations of 1,000 µg/mL for the *F. tenacissima* extract and 215.7 µg/mL for Ag^+ ions in the reaction mixture. The synthesis mixture was then left undisturbed at room temperature for 24 h, allowing the reaction to proceed under ambient conditions.

The successful green synthesis of *Ft*-AgNPs was initially indicated by a distinct color change from pale yellow to reddish-brown, reflecting the surface plasmon resonance (SPR) associated with *Ft*-AgNPs formation. This visual observation was further supported by UV-Visible spectroscopy, which confirmed the formation of *Ft*-AgNPs through the appearance of a characteristic absorption peak. The estimated concentration of the synthesized *Ft*-AgNPs was approximately 215.6 µg/mL. Additional *Ft*-AgNPs concentrations were prepared by adjusting the volumes of $AgNO_3$ and the plant extract to explore concentration-dependent effects in subsequent analysis. The simplicity of the ambient-condition synthesis and the flexibility in reagent ratios underscore the scalability of this green method for broader biomedical and environmental applications. A schematic illustration of the *Ft*-AgNPs synthesis process is presented in Scheme 1.

2.3 Characterization of *Ft*-AgNPs

The absorption characteristics of *Ft*-AgNPs was analyzed using a Cary 60 UV-Vis spectrophotometer (Agilent Technology, United States). The functional groups in the aqueous extract and on the surface of *Ft*-AgNPs were identified using Fourier Transforming Infrared Spectroscopy (FTIR, Agilent Technologies Cary 630) over a range of 4000–400 cm^{-1}. High-performance liquid chromatography (HPLC) analysis of compounds in the aqueous extract of aqueous extract of *F. tenacissima* leaves was conducted using an SPD-20A HPLC system (Shimadzu, Japan) equipped with 254 nm UV detector and RP-C18 column. The X-ray diffraction (XRD) pattern of *Ft*-AgNPs was recorded using an Ultima IV multipurpose X-ray diffractometer (Rigaku, Japan). Morphological characteristics of *Ft*-AgNPs were analyzed with field emission scanning electron microscopy (FESEM, JEOL, SM-IT700HR, Tokyo, Japan). The particle size distribution and average size of *Ft*-AgNPs were determined using High-Resolution Transmission Electron Microscope (TEM, JEOL, JEM-2100f,

United States). Dynamic Light Scattering (DLS) and zeta potential of *Ft*-AgNPs were measured using a Zetasizer Nano ZS (Malvern Instruments, Malvern, United Kingdom).

2.4 Evaluation of antimicrobial activity of *Ft*-AgNPs

The antibacterial efficacy of the aqueous extract of *F. tenacissima* leaves and *Ft*-AgNPs was assessed using the standard disc diffusion method. The following bacterial strains were tested: Gram-positive *B. cereus*, and the Gram-negative *E. coli (ATCC 11775)* and *P. aeruginosa* (*ATCC 9027)*. These strains were maintained on Mueller-Hinton agar at 4°C. Sub-culturing of bacteria was carried out in sterile dishes with uniform depth. The turbidity of bacterial suspensions was adjusted to 0.5 McFarland standard using sterile sodium chloride solution. The bacterial inoculation was performed using a sterile cotton swab to ensure uniform growth with a concentration approximately 10^5–10^6 CFU/mL. Sterile paper discs (6 mm in diameter) were soaked with *Ft*-AgNPs (0.1%; w/v) and placed onto the inoculated agar plates. The plates were incubated at 37°C for 24 h, and the antibacterial activity was evaluated by measuring the zone of inhibition in mm.

The antifungal activity of *Ft*-AgNPs was tested against the yeasts *C. alibicans* and *C. glabrata*. Fungal cultures were grown at 37°C for 24 h in yeast malt broth and then sub-cultured on potato dextrose agar at 35°C for 24 h. Antifungal susceptibility was determined using the disc diffusion method on Mueller-Hinton agar plates.

2.5 Determination of minimum inhibitory concentration (MIC)

MIC of *Ft*-AgNPs was determined as follows: 1 mL of log-phase bacterial culture was mixed with 1 mL of *Ft*-AgNPs and added to 50 mL of sterile nutrient broth, adjusted to pH 6.8. The flasks were incubated in a shaker at 37°C and 140 rpm for 8 h. After incubation, 1 mL of the bacterial culture and *Ft*-AgNPs mixture was serially diluted in sterile saline and spread onto nutrient agar plates. The plates were incubated at 37°C for overnight, and the number of visible colonies on each plate was then counted and recorded.

2.6 Bacterial survival

A mixture of 1 mL of bacterial culture and 1 mL of *Ft*-AgNPs was added to the conical flask containing 50 mL of nutrient broth, while a flask without *Ft*-AgNPs served as the control. All flaks were maintained in a rotary shaker at 150 rpm. At regular intervals, 1 mL samples were withdrawn, mixed with 2 mL of distilled water, and the optical density was measured at 600 nm using a spectrophotometer. Bacterial susceptibility was expressed as survival percentages.

2.7 Evaluation of antioxidant activity

For the evaluation of antioxidant activity, DPPH (2,2-diphenyl-1-picryl-hydrazyl-hydrate) radical scavenging assay was employed. A 4.3 mg/3 mL DPPH stock solution was prepared and subsequently to obtained 5 µg/mL working solution. This working solution was then treated with *Ft*-AgNPs at concentrations ranging from 1–100 µg/mL. The mixtures of *Ft*-AgNPs and DPPH were incubated in the dark for 30 min before measuring absorbance at 517 nm using a UV-Visible spectrophotometer. Pure methanol served as the blank. The antioxidant activity (%) was calculated using the formula:

$$\text{Antioxidant activity } (\%) = \left(A_{control} - A_{sample} / A_{control}\right) \times 100$$

where $A_{control}$ is the absorbance of DPPH alone, and A_{sample} is the absorbance of DPPH and *Ft*-AgNPs mixture.

2.8 Catalytic reduction activity

The catalytic reduction of 4-NP and MB was performed using *Ft*-AgNPs as catalyst. An appropriate amount of *Ft*-AgNPs was added separately to 20 µg/mL solutions of 4-NP and MB. $NaBH_4$ was used as the reducing agent at a concentration equal to or twice that of the pollutant. The reaction mixtures were monitored at 30-min, and the absorption spectra were recorded over a wavelength range of 200–1,000 nm using a UV-visible spectrophotometer.

2.9 Statistical analysis

All experiments were conducted in triplicate. Data analysis was performed using IBM SPSS Statistics version 26 (Armonk, NY, United States). Results are presented as the mean ± standard deviation (SD).

3 Results and discussion

3.1 UV-visible study of plant extract and *Ft*-AgNPs

UV-Visible spectroscopy was employed to analyze the phytochemicals present in the aqueous extract of *F. tenacissima* leaves and to monitor the formation of *Ft*-AgNPs. The UV-Visible spectrum of *F. tenacissima* aqueous leaf extract (Figure 1a) exhibited absorption bands at 254, 221, and 206 nm, which are likely attributed to the presence of hydroxybenzoic acids (HBAs). As secondary metabolites, HBAs are known for their antioxidants, antiviral, anticancer, and antibacterial properties, which may significantly contribute to the reported biological activities of *F. tenacissima* (Assaf et al., 2018; Assaf et al., 2015; Sher et al., 2017; Roy et al., 2017; Singhal et al., 2011; Kirthika et al., 2025; Subramani et al., 2024). Furthermore, the faint yellow (light brown) coloration of the extract was also indicative of HBAs content (Sun et al., 2022). In comparison, the UV-Visible spectrum of $AgNO_3$ displayed an absorption band around 263 nm due to nitrate ions (Mansur and Yahya, 2025), but no SPR peak was detected in the 300–800 nm range.

The UV-Visible spectra of the reaction mixture containing $AgNO_3$ and the aqueous extract of *F. tenacissima* leaves at

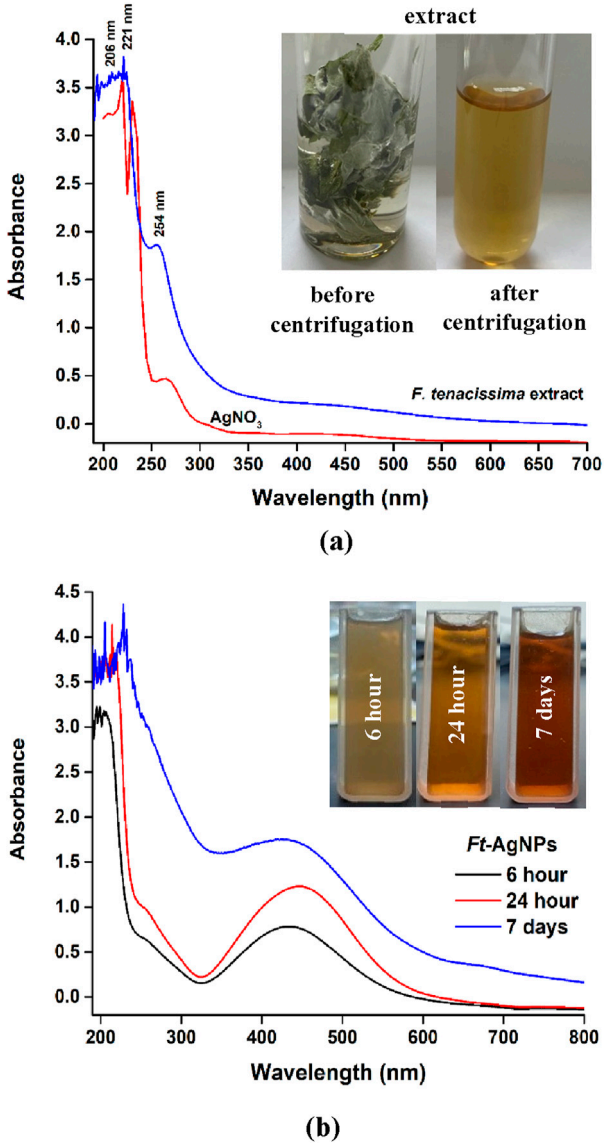

FIGURE 1
(a) UV-Visible spectra of $AgNO_3$ and the aqueous extract of *F. tenacissima* leaves; **(b)** UV-Visible spectra of *Ft*-AgNPs recorded at different time intervals.

different time intervals are presented in Figure 1b. The extract alone appeared faint yellow, but upon mixing with $AgNO_3$, an immediately color change to reddish brown was observed indicating the rapid reduction of Ag^+ ions to Ag^0 and the initial formation of *Ft*-AgNPs. The gradual increase in color intensity over time correlated with *Ft*-AgNPs development, as evidenced by the growing absorbance in the UV-Visible spectra. After 24 h, a well-developed, medium-brown coloration confirmed the successful formation of mature *Ft*-AgNPs. Importantly, the synthesis was carried out entirely at room temperature without the need for external heating or agitation, supporting the energy efficient and environmental friendliness of the process. The resulting *Ft*-AgNPs remained colloidally stable for up to 7 days, showing only minimal changes in the UV-Visible peak profile, which indicated limited aggregation. *Ft*-AgNPs obtained after 24-h time point were selected for subsequent antimicrobial, antioxidant, and catalytic activity evaluations. This green synthesis approach demonstrates strong scalability potential, owing to its uncomplicated room-temperature procedure and the ease with which reagent ration can be modified.

3.2 FTIR analysis of plant extract and *Ft*-AgNPs

FTIR analysis was performed in the range of 4000–400 cm^{-1} to identify the phytochemicals present in the aqueous extract of *F. tenacissima* leaves and attached to the surface of *Ft*-AgNPs. The resulting FTIR spectra are shown in Figure 2a, where the characteristics peaks of *F. tenacissima* (red spectrum) can be distinguished from those of *Ft*-AgNPs (blue spectrum). The stretching vibration of the C=O bond, observed at 1766 cm^{-1} in the plant extract, was slightly red-shifted and reduced in intensity in the *Ft*-AgNPs spectrum, indicating electrostatic interactions between the C=O group and Ag^+ ions. The band at 1,589 cm^{-1}, corresponding to the C=C stretching vibration of the aromatic ring, was blue-shifted in the *Ft*-AgNPs spectrum with reduced intensity, suggesting a decrease in conjugation (Andreani et al., 2019; Alfei et al., 2022). The reduction of Ag^+ ions likely occurred via the oxidation of phenolic -OH groups to ketonic C=O, but intriguingly, the higher-frequency C=O stretching vibration did not appear in the *Ft*-AgNPs spectrum, indicating that the ketonic C=O group acted as a stabilizing agent (discussed further in the synthesis mechanisms) (Bashami et al., 2018).

The O-H stretch vibration was observed at 3338 cm^{-1}, while the O-H bending appeared at 1,114 cm^{-1}. The absorption band at 3462 cm^{-1} confirmed the presence of carboxylic group in the compound (Andreani et al., 2019; Alfei et al., 2022). The carboxylic group also exhibited a C-O stretch at 13498 cm^{-1}, and the C-O stretch of alcohol was observed at 993 cm^{-1}. The peak at 842 cm^{-1} was attributed to the C-H bending of aromatic hydrocarbons, while the peaks at 1,299 and 1,238 cm^{-1} indicated C-C stretching (Bashami et al., 2018). Furthermore, the shifting and broadening of the peak from 661 cm^{-1} to 696 cm^{-1} suggested the formation of Ag_2O (Edayadulla and Sundari, 2024). These identified functional groups strongly indicated the presence of HBAs in the aqueous extract of *F. tenacissima* leaves. These same functional groups were also present in the FTIR spectrum of *Ft*-AgNPs, albeit, with minor differences. Thus, these functional groups played a key role in both the reduction and stabilizing of *Ft*-AgNPs in the aqueous solution. The FTIR results support the mechanism outlined in Scheme 2.

3.3 HPLC analysis of the aqueous extract of *F. tenacissima* leaves

HPLC analysis of the aqueous extract of *F. tenacissima* leaves was performed using an acetonitrile:acetic acid (50:50) mobile phase and RP-C18 column to identify and confirm the presence of HBAs responsible for reducing Ag + ion and stabilizing *Ft*-AgNPs. The chromatogram shown in Figure 2b, revealed two major peaks at retention times of 2.07 and 2.63 min. These retention times were

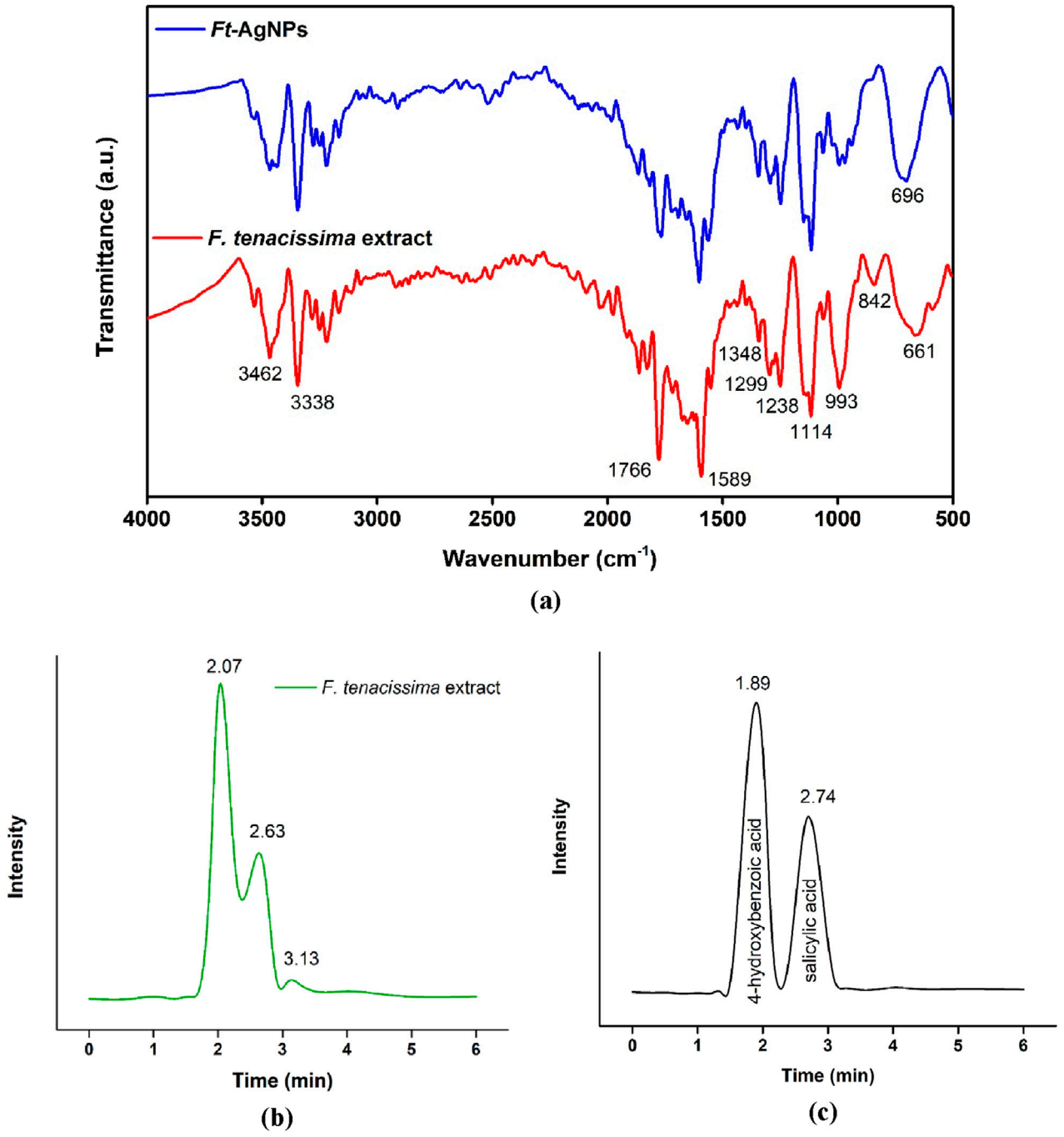

FIGURE 2
(a) FTIR spectra of the aqueous extract of *F. tenacissima* leaves (red) and *Ft*-AgNPs (blue), **(b)** HPLC spectra of the aqueous extract of *F. tenacissima* leaves, and **(c)** standard 4-hydroxybenzoic acid and 2-hydroxybenzoic acid (salicylic acid).

compared with standards of 4-hydroxybenzoic acid and salicylic acid (2-hydroxybenzoic acid), as shown in Figure 2c. The retention times of 4-hydroxybenzoic acid and salicylic acid were found to be 2.01 and 2.59 min, respectively, closely matching the retention times of compounds found in the aqueous extract of *F. tenacissima* leaves (Shah et al., 2013; Desai and Senta, 2015), confirming the presence of 4-hydroxybenzoic acid and salicylic acid. Additionally, a third, less prominent peak at 3.14 min was observed, which may correspond to trace amounts of other phenolic compounds. Overall, the HPLC analysis validated the presence of 4-hydroxybenzoic acid and salicylic acid as the primary constituents in the aqueous extract of *F. tenacissima* leaves.

3.4 Synthesis mechanism of *Ft-AgNPs*

The proposed mechanism for the synthesis of *Ft*-AgNPs is illustrated in Scheme 2. The highly reactive phenolic -OH group

10.3389/fnano.2025.1587084

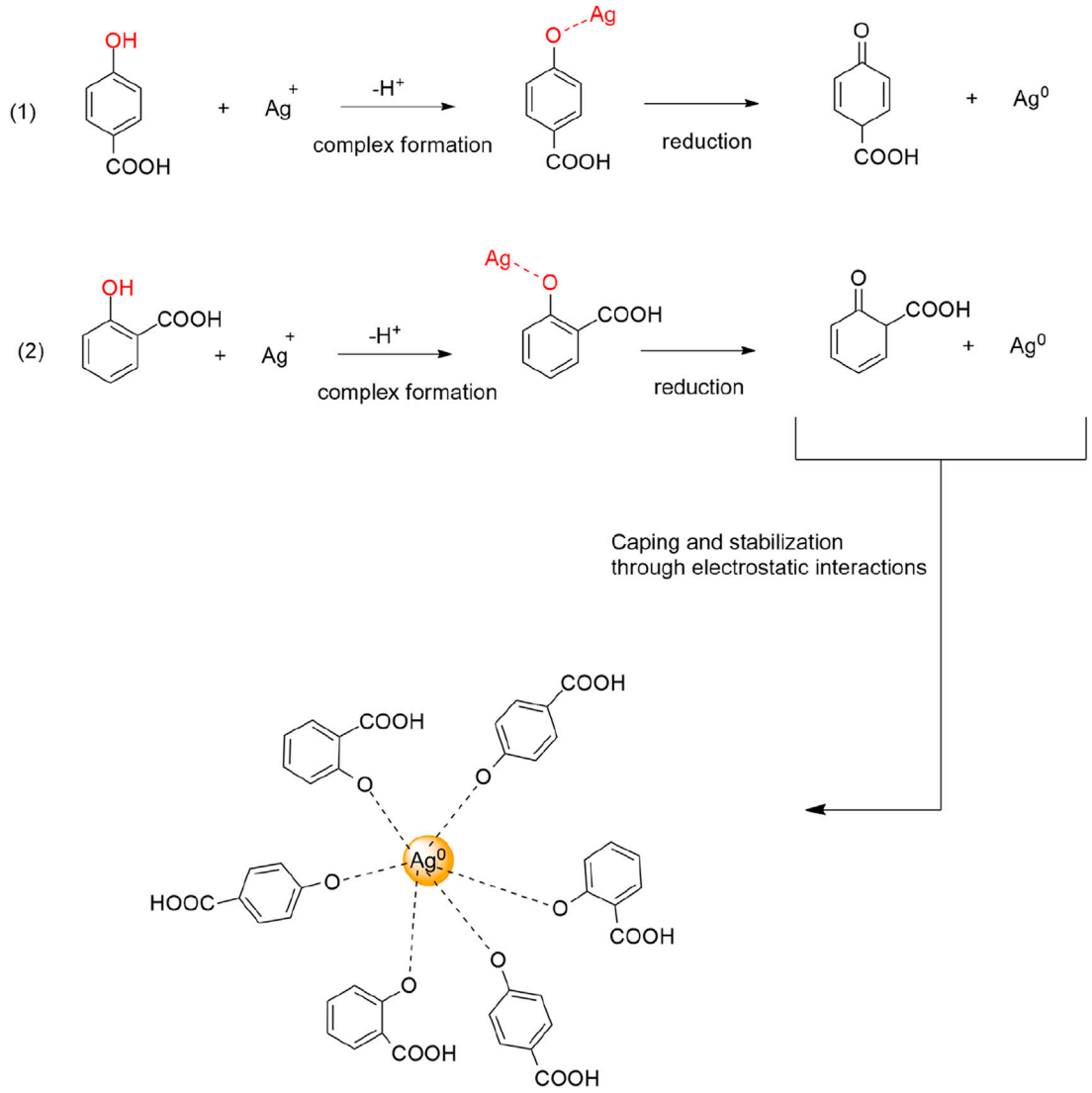

SCHEME 2
Proposed synthesis mechanism of *Ft*-AgNPs and stabilization by oxidized hydroxybenzoic acids derivatives.

of 4-hydroxybenzoic acid (or salicylic acid) present in the plant extract plays a crucial role in the reduction of Ag^+ ions to metallic Ag^0, thereby initiating the formation of *Ft*-AgNPs through a single electron transfer process (Liu et al., 2018). During this reaction, the phenolic compound is oxidized to a corresponding quinonoid structure. In addition to acting as a reducing agent, the oxidized form of 4-hydroxybenzoic acid (or salicylic acid) also contributes to *Ft*-AgNPs stability by binding to the surface of the newly formed *Ft*-AgNPs, preventing their aggregation. This surface stabilization, often referred to as surface passivation (Khan et al., 2022), is a critical feature of synthesized *Ft*-AgNPs. The phytochemicals not only cap the AgNPs surface but also form a bio-organic shell that maintains the colloidal stability of *Ft*-AgNPs over time. This shell provides both steric hindrance and electrostatic repulsing, reducing the likelihood of particle agglomeration and enhancing dispersion in aqueous environments. Importantly, this natural capping layer also plays a significant role in limiting the uncontrolled release of Ag^+ ions and improving the biocompatibility of the *Ft*-AgNPs. These collective factors likely contribute to the minimal cytotoxic effect that will be observed for the synthesized *Ft*-AgNPs.

3.5 X-ray diffraction analysis of *Ft*-AgNPs

The XRD analysis of *Ft*-AgNPs was performed, and the resulting spectrum is shown in Figure 3. Several sharp, crystalline peaks were observed, with four major prominent peaks at 2θ = 40.3°, 45.95°, 63.24°, and 76.95°. These peaks corresponded to the reflection planes of (111), (200), (220), and (311), confirming the face-centered cubic (fcc) structure of Ag (Mughal et al., 2024). Additionally, an intense peak at 2θ = 32.7° was detected, which aligns with the XRD data of Ag_2O, representing the formation of Ag_2O due to exposure to atmospheric oxygen during the drying process. Some unassigned peaks (marked with stars) were also observed, which may indicate the crystallization of bio-organic components on the surface of the *Ft*-AgNPs.

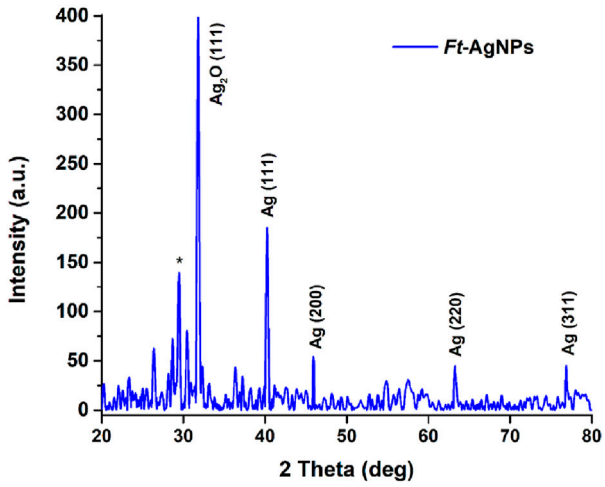

FIGURE 3
XRD pattern of *Ft*-AgNPs.

3.6 SEM images of *Ft*-AgNPs

The shape, aggregation, and dispersibility of *Ft*-AgNPs were analyzed using SEM. Samples were prepared on a silicon water, and the SEM images at magnifications of (a) 30,000x, (b) 60,000x, and (c) 120,000x are presented in Figures 4a–c. The images clearly showed the presence of densely packed *Ft*-AgNPs, with individual particles predominantly spherical in shape, though some minimal aggregation was observed. The aggregation of smaller particles into larger ones may be attributed to the influence of secondary HBAs present in the leaf extract. At higher magnifications, the *Ft*-AgNPs were uniformly dispersed across the substrate surface, exhibiting adequate porosity, which is beneficial for inhibiting biofilm formation (Nwabor et al., 2021). The average particle size of the *Ft*-AgNPs was found to be less than 10 nm, as confirmed by TEM analysis. Given that smaller nanoparticles have a greater surface area for interaction with bacterial cells, the *Ft*-AgNPs are expected to exhibit high antimicrobial activity due to their enhanced ability to interact with bacterial surfaces. Additionally, the HBAs attached to the surface of *Ft*-AgNPs play a crucial role in bringing the *Ft*-AgNPs into close proximity to bacterial surfaces, facilitating their internalization.

3.7 Particle size determination of *Ft*-AgNPs using TEM

The particle size distribution and average particle size of *Ft*-AgNPs were determined using TEM analysis. A colloidal solution of *Ft*-AgNPs was directly deposited onto a carbon tape substrate and air-dried before being examined. The TEM images obtained at magnifications of 100,000x and 150,000x, shown in Figures 5a,b, revealed well-shaped, uniformly dispersed *Ft*-AgNPs with no aggregation. Smaller particles were found to be more abundant, with the majority of the particles falling within the size range of 2–18 nm, as illustrated in Figure 5c. Gaussian fitting of the size distribution yielded a mean particle size of 9.8 ± 0.1 nm, which aligns well with the SEM results. These findings suggest that the aqueous extract of *F. tenacissima* leaves is effective in producing stable, uniform, and highly dispersed spherical *Ft*-AgNPs with an average size less than 10 nm. This study is novel, as it represents the first report of *Ft*-AgNPs synthesis using *F. tenacissima* leaves.

3.8 Zeta potential and DLS

Zeta potential and DLS measurements were carried out to determine the surface charge and particle size distribution of *Ft*-AgNPs. The zeta potential, a key indicator of colloidal stability, was measured at −24.1 ± 1 mV for *Ft*-AgNPs (Paseban et al., 2019). A higher charge indicates greater stability in the colloidal solution due to stronger repulsive forces between the particles, while a lower charge suggests a tendency for aggregation (Paseban et al., 2019; Sánchez et al., 2016). The negative zeta potential further suggests that the surface of *Ft*-AgNPs is functionalized with oxidized derivatives of HBAs. The particle size distribution obtained from the DLS measurements is shown in Figure 5d. Although DLS is an intensity-based technique that typically highlights larger particles (Gonzalez-Fuenzalida et al., 2016), the majority of the *Ft*-AgNPs synthesized from the aqueous extract of *F. tenacissima* leaves were small and displayed no aggregation. Consequently, the DLS particle size distribution aligned well with the TEM results, indicating an average particle size of 12.1 ± 0.1 nm.

3.9 Antimicrobial efficacy of *Ft*-AgNPs

The antibacterial activity of $AgNO_3$, aqueous extract of *F. tenacissima* leaves, and *Ft*-AgNPs against *B. cereus*, *E. coli*, and *P. aeruginosa* was evaluated using the disc diffusion method (N et al., 2024). The susceptibility of the selected bacteria to *Ft*-AgNPs was assessed based on the diameters of zones of inhibition (mm). The results of the disc diffusion experiments are shown in Figures 6a–c. The bacteria (a) *B. cereus* (b) *E. coli*, and (c) *P. aeruginosa* were treated with (1) ~20 µg/mL *Ft*-AgNPs, (2) ~20 µg/mL $AgNO_3$, and (3) ~20 µg/mL aqueous extract of *F. tenacissima* leaves, respectively. As seen, *Ft*-AgNPs produced a significant zone of inhibition, while no zones of inhibition were observed for $AgNO_3$ and aqueous extract of *F. tenacissima* leaves against the selected bacteria. This suggests that the aqueous solution of $AgNO_3$ solution and aqueous extract of *F. tenacissima* leaves were ineffective in killing the bacteria. In contrast, the similar concentration of *Ft*-AgNPs produced zones of inhibition ranging 12–14 mm in diameter. The stronger antibacterial effects of *Ft*-AgNPs were attributed to their small size, large surface area, and functionalized surface, which enable enhanced physical interactions with bacterial surfaces. These interactions likely result in disruption of the bacterial cell wall and internalization of *Ft*-AgNPs, ultimately causing damage to the intracellular components of the bacterial cell. Furthermore, the disc diffusion assay revealed that *B. cereus* and *P. aeruginosa* were more susceptible to *Ft*-AgNPs than *E. coli*.

The dose-dependent antibacterial effects of *Ft*-AgNPs were evaluated across a concentration range of 10–50 µg/mL. The zone of inhibition produced by 20 µg/mL of *Ft*-AgNPs is shown in Figures 6a–c, while the zones of inhibition for (a) 10, (b) 30, (c) 40,

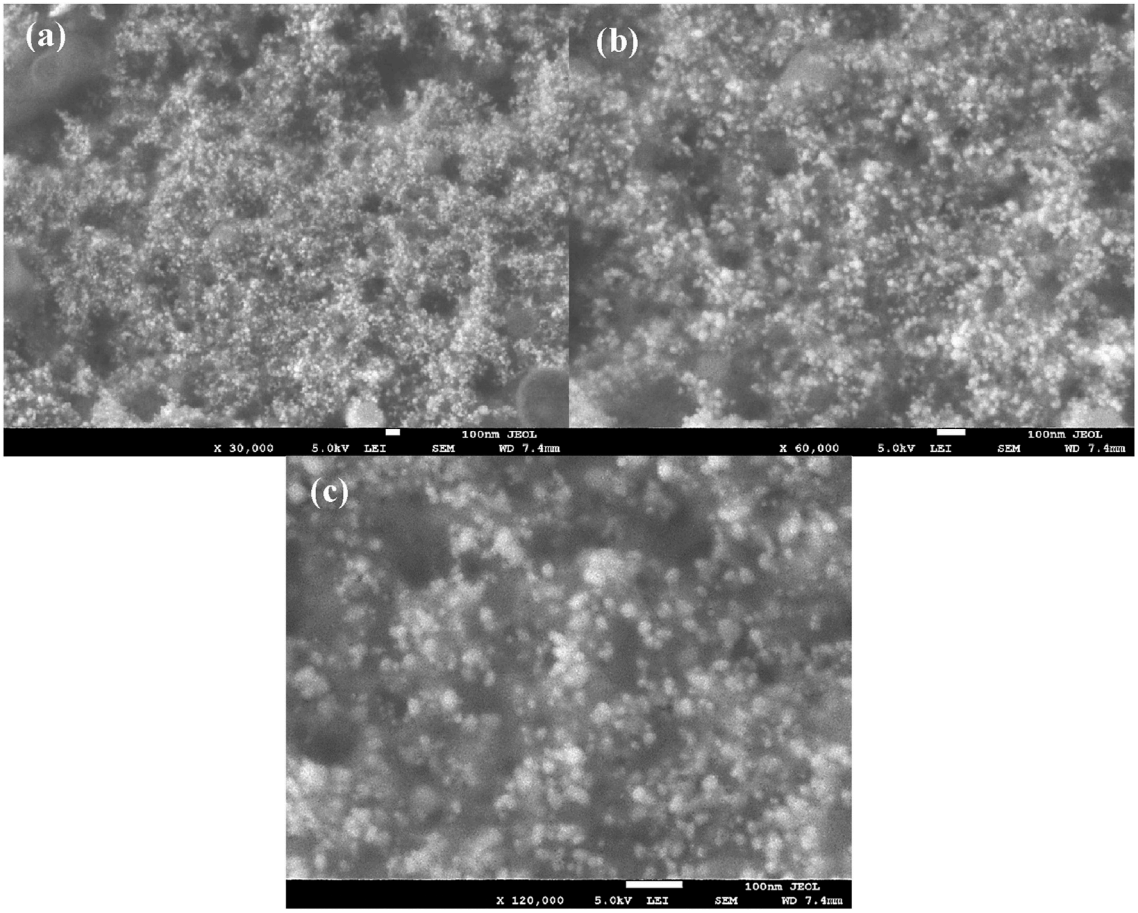

FIGURE 4
SEM images of *Ft*-AgNPs at magnification of **(a)** ×30,000, **(b)** 60,000x, and **(c)** 120,000x.

and (d) 50 μg/mL *Ft*-AgNPs are presented in Figure 7a for the same bacterial strains. The corresponding diameters of the zones of inhibition are provided in Table 1. As the concentration of *Ft*-AgNPs increased, an enhancement in bacterial susceptibility was observed for all three stains. Notably, *B. cereus* and *E. coli* exhibited greater sensitivity to the concentration variation of *Ft*-AgNPs compared to *P. aeruginosa*. Nevertheless, the antibacterial activity of *Ft*-AgNPs clearly improved with higher concentrations, indicating that larger doses were more effective in eliminating bacterial infections caused by the tested strains. Consequently, *Ft*-AgNPs demonstrated bacteriostatic behavior at low concentrations and bactericidal effects at higher concentrations. The overall antibacterial efficacy of *Ft*-AgNPs followed the order: *P. aeruginosa* < *E. coli* < *B. cereus*. Therefore, *Ft*-AgNPs within the concentration range of 10–50 μg/mL were found to be sufficiently potent to effectively combat bacterial infections without inducing toxic effects.

The antifungal activity of *Ft*-AgNPs was evaluated against two yeast species, *C. albicans* and *C. glabrata* using *Ft*-AgNPs concentrations of 20, 40, and 100 μg/mL. The results are presented in Figures 7b,c. Remarkably, *Ft*-AgNPs exhibited strong antifungal effects, surpassing their antibacterial performance, with zones of inhibition ranging from 19 to 24 mm. This enhanced activity is likely attributed to the structure of fungal cell walls, which although thicker than bacterial cell walls, are more porous due to their composition of chitin and β-glucans (Feofilova, 2010). This porous nature facilitates easier penetration of *Ft*-AgNPs into fungal cells compared to the denser, peptidoglycan-rich walls of bacteria. The highest antifungal activity against both yeast species was achieved at 40 μg/mL of *Ft*-AgNPs. However, at a higher concentration of 100 μg/mL, the antifungal efficiency decreased, likely due to nanoparticles aggregation. Overall, *Ft*-AgNPs in the concentration range of 10–50 μg/mL, consistent with the antibacterial findings, demonstrated excellent antifungal activity against the tested fungal strains.

While AgNPs are widely acceptable for their strong antimicrobial efficacy, their interaction with human cells and over biocompatibility remain key concerns, particularly for biomedical use. Cytotoxicity refers to the potential of AgNPs to harm healthy mammalian cells, not just target microbial pathogens (Tripathi and Goshisht, 2022). Therefore, it is important to assess both the cytotoxicity and biocompatible behavior of the green synthesized *Ft*-AgNPs. The cytotoxic profile of *Ft*-AgNPs is influenced by several parameters, including particle size, shape, surface chemistry, concentration, dosage, and duration of exposure (Khan et al., 2022). These characteristics directly impact the release of Ag^{+} ions in biological environments, a process widely

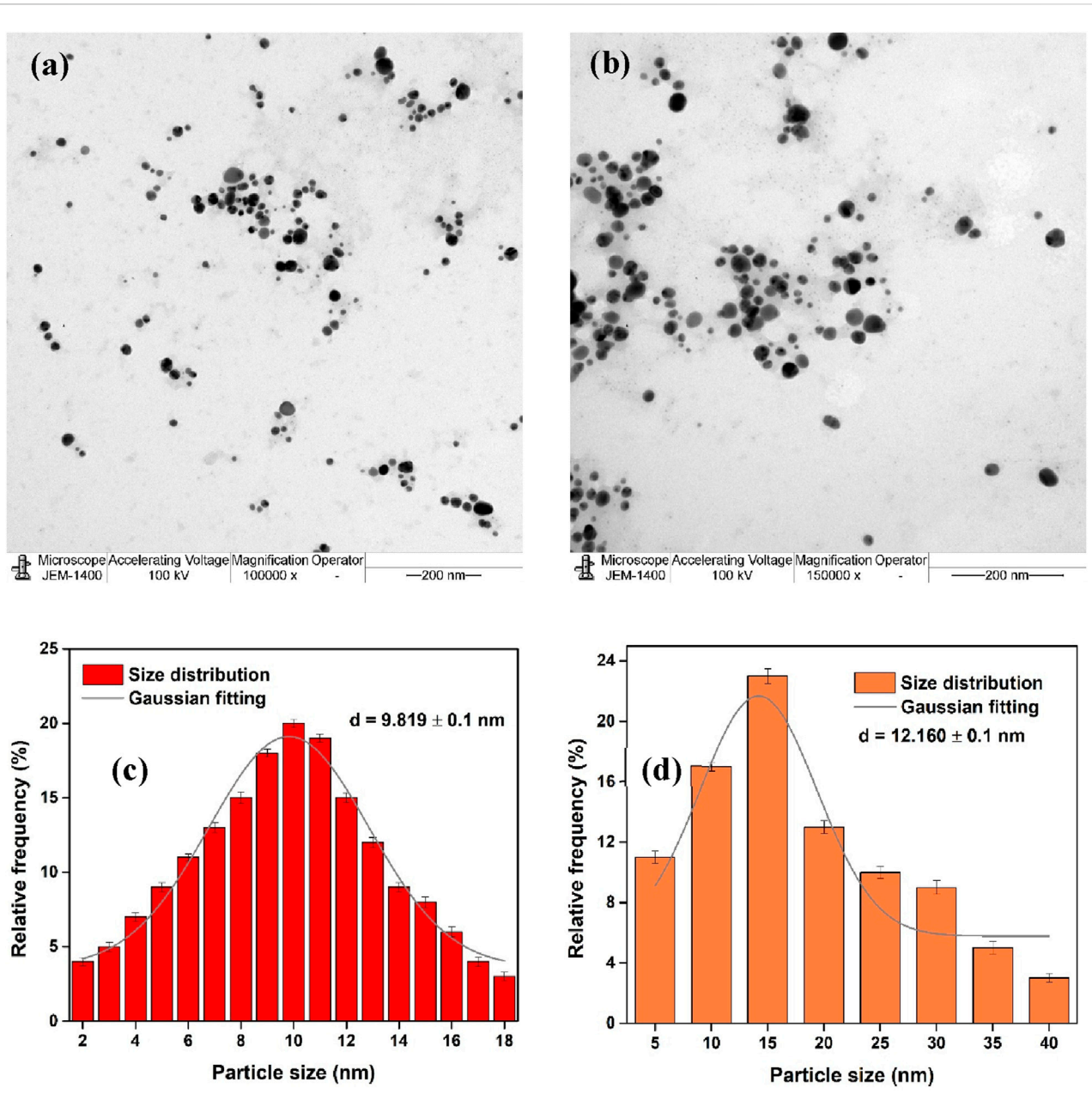

FIGURE 5
TEM images of *Ft*-AgNPs at magnifications of **(a)** ×100,000 and **(b)** ×150,000 magnification; **(c)** particle size distribution derived from TEM analysis; and **(d)** particle size distribution obtained from DLS analysis.

acknowledged as the main contributor to AgNPs-induced toxicity. Notably, AgNPs synthesized via green methods tend to release Ag^+ at a slower rate and are generally considered less toxic than their uncapped or chemically synthesized counterparts (Khan et al., 2022).

Among the aforementioned factors, concentration is another critical factor. Literature reports indicate that AgNPs at concentrations below 10 μg/mL typically show minimal toxicity, while levels between 10–50 μg/mL may cause moderate effects. Concentrations exceeding 100 μg/mL are associated with significant cytotoxic outcomes, such as mitochondrial impairment, programmed cell death (apoptosis or necrosis) and the overproduction of ROS species (Khan et al., 2022; Kirthika et al., 2025; Subramani et al., 2024). Neverthelss, green synthesized AgNPs, particularly those produced using plant extracts, have demonstrated consistently low cytotoxicity (Khan et al., 2022; Kirthika et al., 2025; Subramani et al., 2024). This is largely due to the presence of natural phytochemicals that act as both reducing and stabilizing agents, resulting in the formation of a bio-organic layer on the AgNPs surface. This organic shell not only enhances stability but also reduces direct Ag^+ ion toxicity, contributing to improved biocompatibility.

Thus, the cytotoxicity of *Ft*-AgNPs is context-specific and can be modulated by adjusting their physiochemical features and synthesis conditions. Since green synthesis inherently provides surface passivation (stabilization) through phytochemical coatings and

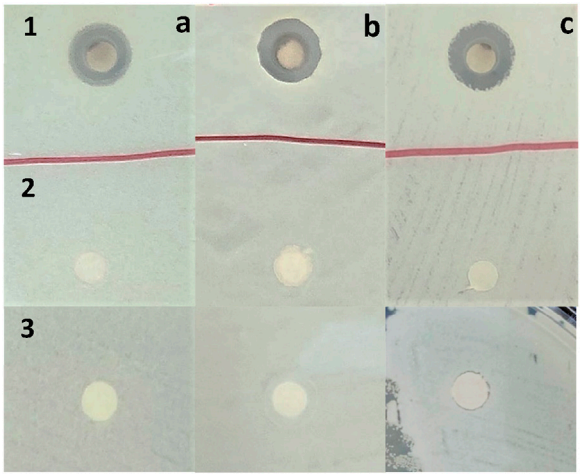

FIGURE 6
Disc diffusion experiment results showing the antibacterial susceptibility of **(a)** *B. cereus*, **(b)** *E. coli*, and **(c)** *P. aeruginosa* to (1) ~20 µg/mL *Ft*-AgNPs, (2) ~20 µg/mL $AgNO_3$, and (3) ~20 µg/mL aqueous extract of *F. tenacissima* leaves, respectively.

moderates Ag^+ ion release, the *Ft*-AgNPs presented in this study are anticipated to exhibit low to moderate cytotoxicity, as the concentration used were below 50 µg/mL, along with favorable biocompatibility, both essential attributes for their prospective biomedical applications. To establish the safety of green synthesized *Ft*-AgNPs, the following evaluations are recommended: *in vitro* cytotoxicity assays such as MTT, LDH release, and ROS generation studies using human cell lines.

3.10 MIC determination using the colony forming unit (CFU) method

Minimum inhibitory concentration (MIC) refers to the lowest concentration of an antimicrobial agent that prevents visible bacterial growth. In this study, the MIC of *Ft*-AgNPs against *B. cereus* and *E. coli* was determined using the CFU method (Sieuwerts et al., 2008), which involves quantifying the number of viable bacteria. As shown in Figure 8a, a bacterial stock solution was spread onto agar plates, where each visible colony originated from a single viable bacterial cell. The CFU was calculated by counting the number of bacterial colonies on the agar plates and determining the number colonies per unit volume of the original stock solution. Serial dilution of *Ft*-AgNPs resulted in concentrations ranging from 0to 10.5 µg/mL.

At 0 µg/mL *Ft*-AgNPs concentration, the CFU counts for both *B. cereus* and *E. coli* were high. However, as the *Ft*-AgNPs concentration increased, a gradual decrease in CFU was observed, reaching nearly zero for *B. cereus* at 8.4 µg/mL, and for *E. coli* at 10.5 µg/mL. As shown in Figures 8b,c and Table 2 , 2.1 µg/

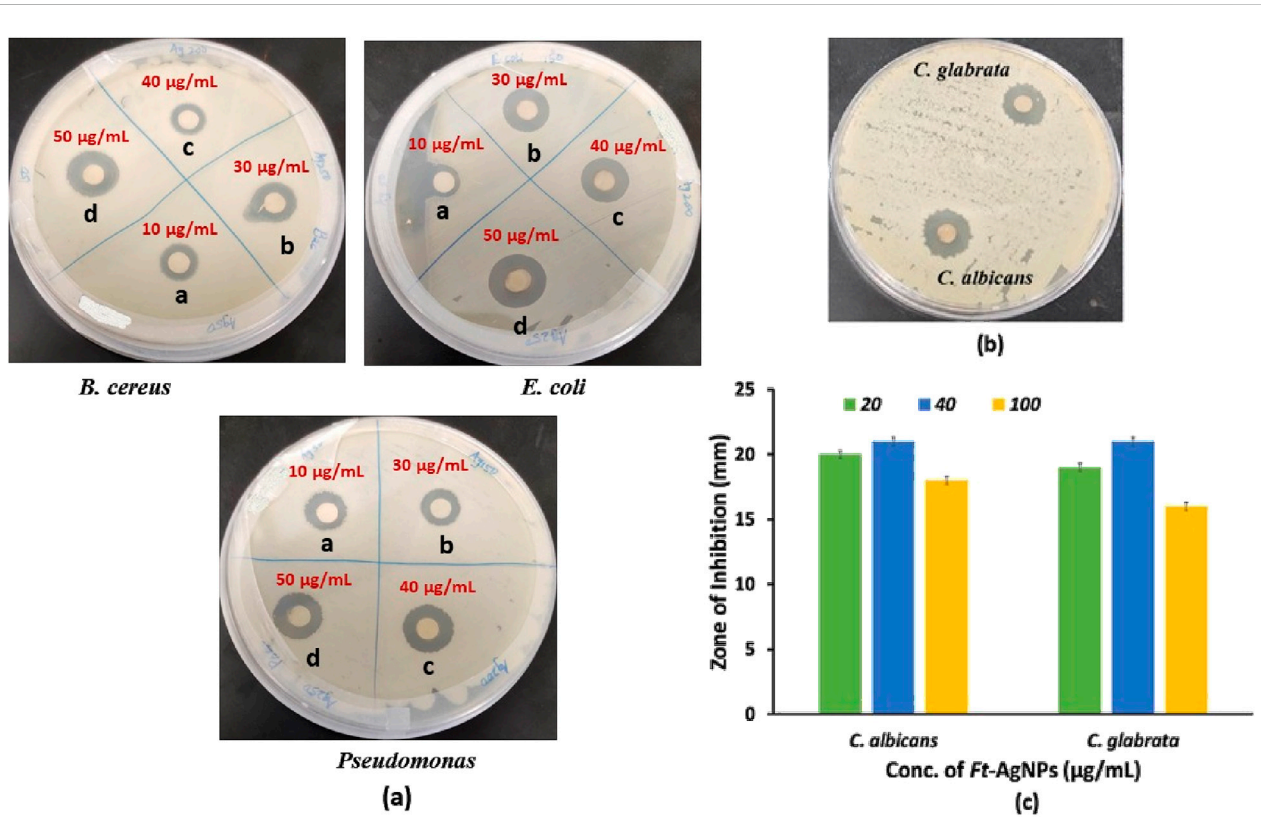

FIGURE 7
(a) Does-dependent antibacterial activity of *Ft*-AgNPs, **(b)** Zone of inhibition formed by *Ft*-AgNPs against *C. albicans* and *C. glabrata*, and **(c)** concentration-dependent antifungal activity of *Ft*-AgNPs.

10.3389/fnano.2025.1587084

TABLE 1 Zone of inhibition diameters produced by *Ft*-AgNPs against selected bacteria.

Ft-AgNPs (μg/mL)	*B. cereus*	*E. coli*	*P. aeruginosa*
	Diameter in mm		
10	13 ± 0.3	11 ± 0.1	13 ± 0.1
20	14 ± 0.2	12 ± 0.3	14 ± 0.1
30	15 ± 0.3	16 ± 0.1	14 ± 0.3
40	17 ± 0.4	16 ± 0.4	16 ± 0.2
50	19 ± 0.1	19 ± 0.2	16 ± 0.4
Ciprofloxacin (30 μg/mL)	25 ± 0.5	26 ± 0.4	30 ± 0.7

mL of *Ft*-AgNPs was identified as the minimum concentration capable of visibly inhibiting the growth of both bacteria. Compared to values reported in the literature, the MIC of *Ft*-AgNPs against *B. cereus* and *E. coli* appears slightly lower. The MIC_{50} of *Ft*-AgNPs, defined as the concentration at which 50% of bacterial cells are inhibited, was determined using linear regression analysis of log(CFU/mL) vs. concentration (μg/mL) data and was found to be 3.94 μg/mL for both bacteria. Notably, the MIC_{50} values of *Ft*-AgNPs are slightly higher but remain comparable to the MIC_{50} values reported for ciprofloxacin (0.125 μg/mL) against *B. cereus* and *E. coli* by the disc diffusion method (Smith et al., 1988; Cohen et al., 1991). Additionally, the minimum bactericidal concentration (MBC), defined as the concentration required to kill 99.99% of the bacteria, was determined using the CFU method. The MBC corresponded to the *Ft*-AgNPs that reduced CFU counts to fewer than 30 colonies per mL, specifically 8.4 μg/mL for *B. cereus* and 10.5 μg/mL for *E. coli*, respectively. The MIC analysis clearly demonstrated that the *F. tenacissima*-derived *Ft*-AgNPs hold considerable promise as an effective alternative antimicrobial agent against majority of bacterial and fungal stains.

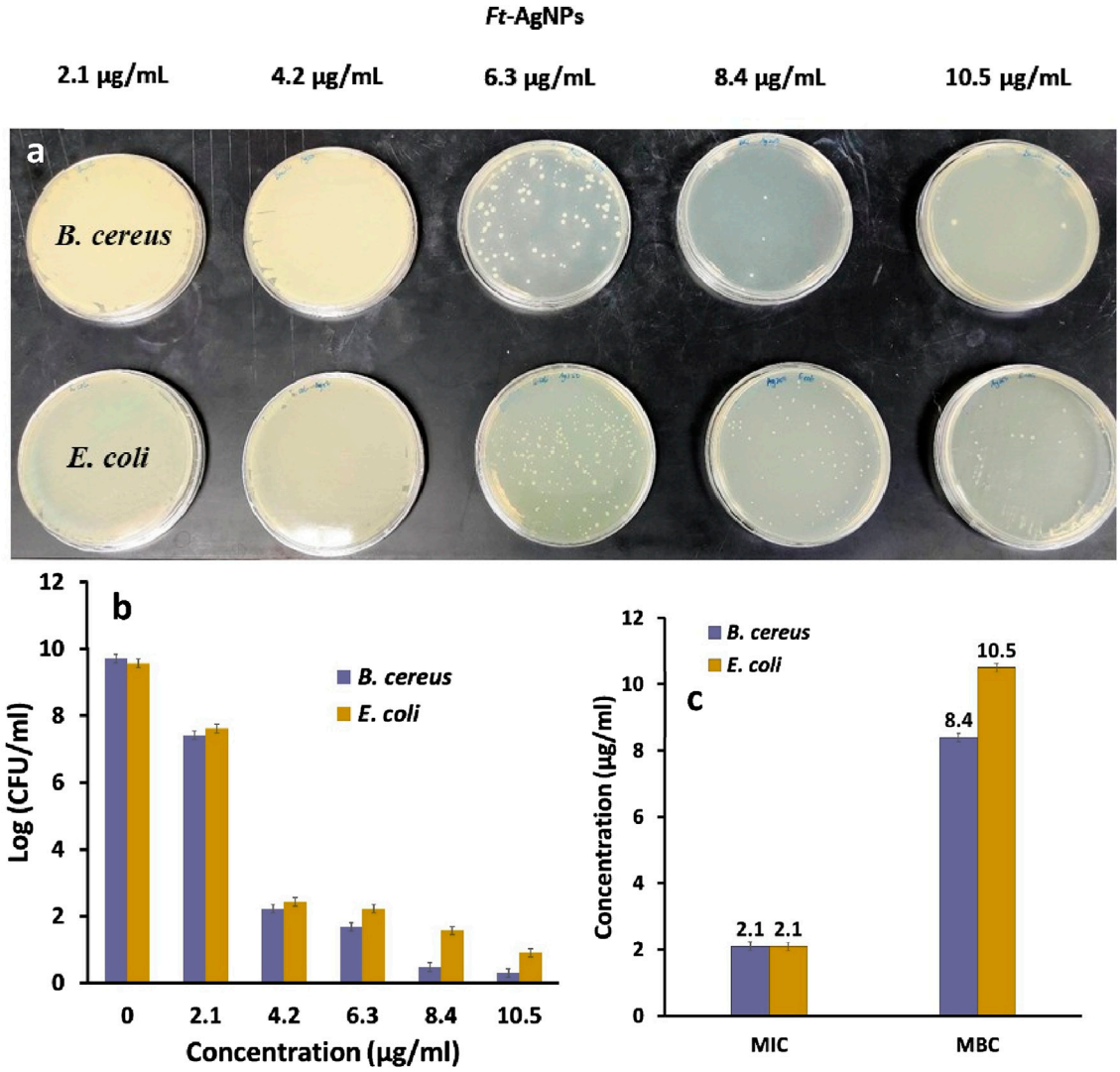

FIGURE 8
(a) Determination of the MIC of *Ft*-AgNPs using CFU method, **(b)** plot of log(CFU/mL) *versus Ft*-AgNPs concentration, and **(c)** MIC and MBC value of *Ft*-AgNPs against *B. cereus* and *E. coli*.

10.3389/fnano.2025.1587084

TABLE 2 MIC and MBC values of *Ft*-AgNPs against selected bacteria.

Ft-AgNPs (μg/mL)	*B. cereus* (CFU/mL)	*E. coli* (CFU/mL)
0	$52 \times 10^8 \pm 1.1$	$37 \times 10^8 \pm 1$
2.1	$26 \times 10^6 \pm 1.2$	$41 \times 10^6 \pm 1.2$
4.2	$2.1 \times 10^3 \pm 1$	$4.7 \times 10^3 \pm 1.22$
6.3	48 ± 1.1	169 ± 1.1
8.4	3 ± 1.3	37 ± 1.2
10.5	2 ± 1.25	8 ± 1.1

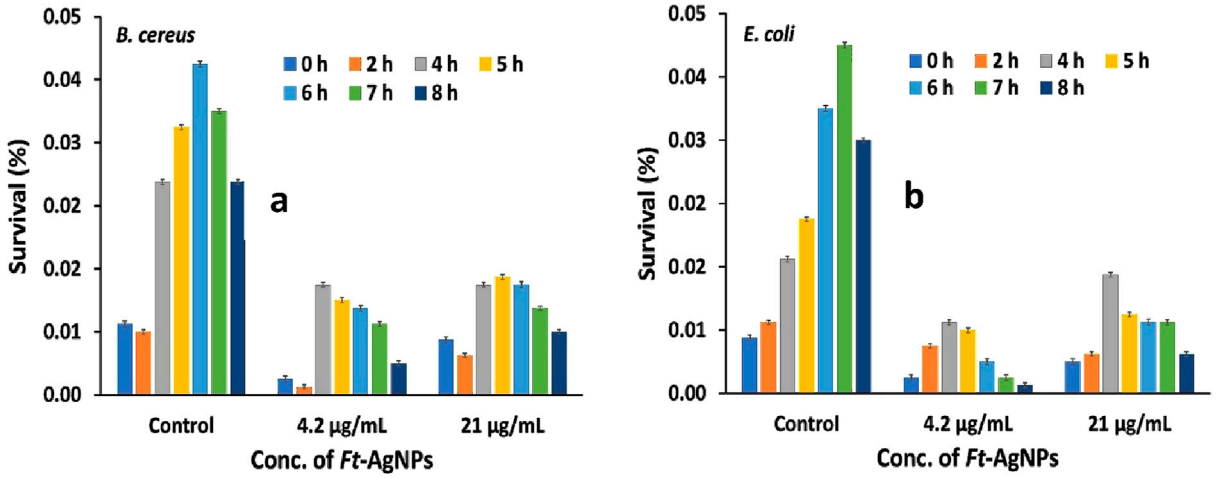

FIGURE 9
Survival (%) of **(a)** *B. cereus* and **(b)** *E. coli* following treatment with *Ft*-AgNPs.

3.11 Bacterial survival study against *Ft*-AgNPs

The survival of *B. cereus* and *E. coli* was also assessed following treatment with two concentrations of *Ft*-AgNPs, alongside an untreated control (Katzenberger et al., 2021). The absorbance of *Ft*-AgNPs-treated bacterial suspensions was recorded at regular intervals, and the data were expressed as survival percentages, as shown in Figures 9a,b. Compared to the control, *Ft*-AgNPs significantly inhibited the growth of both bacterial strains, confirming their promising antibacterial potential. Interestingly, when comparing the two *Ft*-AgNPs concentrations, bacterial survival was higher at 21 μg/mL than at 4.2 μg/mL. This counterintuitive trend may be attributed to increased *Ft*-AgNPs aggregation at higher concentrations, which could reduce surface availability and limit direct interaction between the *Ft*-AgNPs and bacterial cells, thereby diminishing their antimicrobial efficiency.

Moreover, *E. coli* exhibited a more rapid decline in viability compared to *B. cereus*, indicating a higher sensitivity to *Ft*-AgNPs exposure over time. This trend aligns with the disk diffusion assay results, which also showed pronounced susceptibility of both bacteria to *Ft*-AgNPs. Overall, the survival study revealed that *B. cereus* exhibited a slightly greater resistance to prolonged *Ft*-AgNPs treatment compared to *E. coli*, indicating a strain specific variation in susceptibility to the *Ft*-AgNPs.

3.12 Proposed mechanism of antimicrobial activity

The antimicrobial activity of AgNPs has been reported to occur through multiple synergistic pathways (Khan et al., 2022; Kirthika et al., 2025; Subramani et al., 2024). These include disruption of the microbial cell membrane, which was achieved through physical attachment of AgNPs to the cell surface, increasing membrane permeability and resulting in the leakage of intracellular contents. Biofilm formation was inhibited as AgNPs prevented microbial adhesion, disrupted mature biofilms, and penetrated the extracellular matrix. Following internalization, AgNPs were found to interact with intracellular components such as ribosomes and DNA, thereby inhibiting protein synthesis and replication processes. Furthermore, the generation of ROS species, including superoxide anion and hydroxyl radicals, was catalyzed, leading to oxidative damage of lipids, proteins, and nucleic acids. Ag^+ ions, released from the AgNPs surface, were shown to bind to membrane proteins and essential enzymes, thereby impairing respiration and disrupting

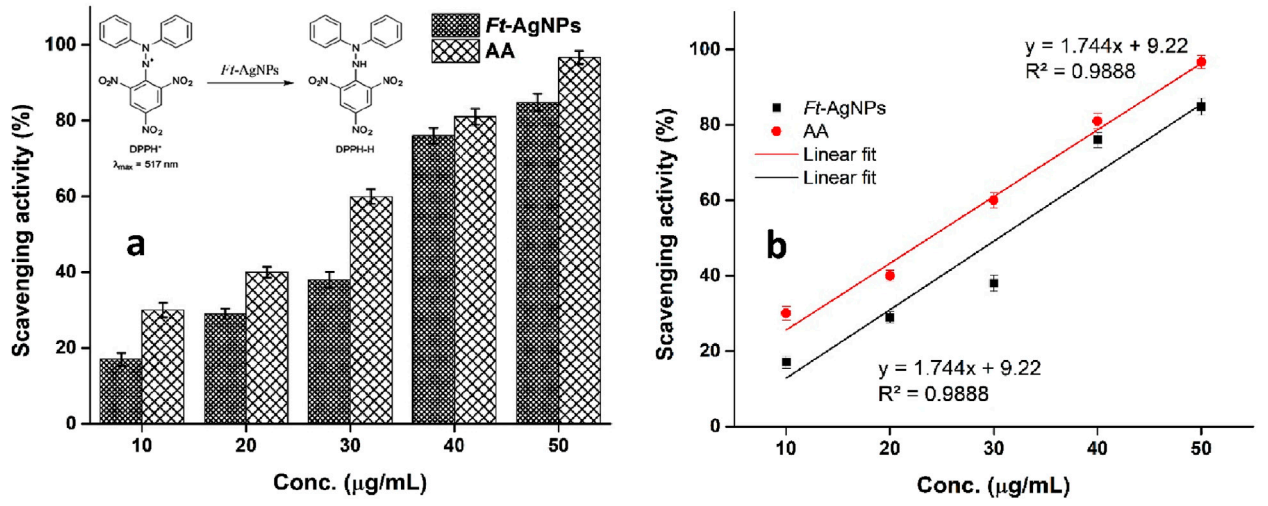

FIGURE 10
(a) Comparative analysis of antioxidant activity of *Ft*-AgNPs and AA using the DPPH assay and **(b)** linear regression analysis of the same.

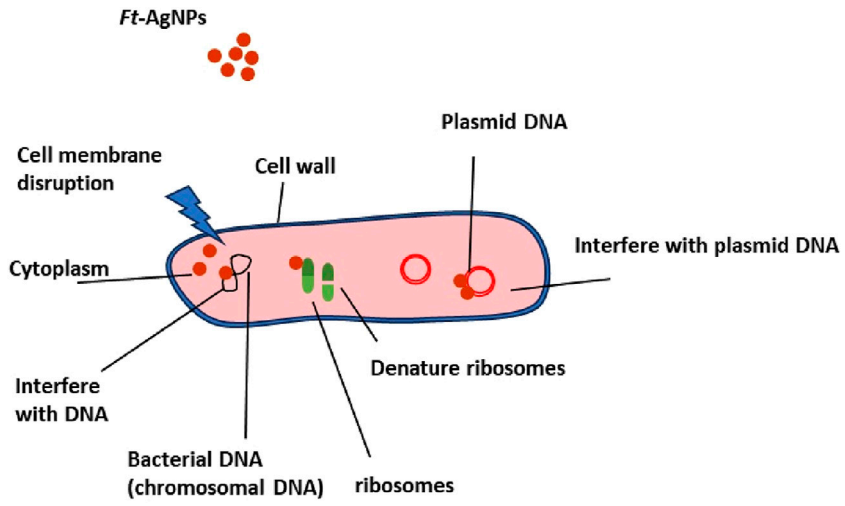

SCHEME 3
Schematic representation of bacterial or fungal cell damage induced by *Ft*-AgNPs.

cellular metabolism (Khan et al., 2022; Kirthika et al., 2025; Subramani et al., 2024). Together, these effects contributed to the overall antimicrobial action.

In the case of *Ft*-AgNPs, the antimicrobial mechanism was understood to occur also in two major stages: an initial physical interaction with the microbial cell membrane, followed by internalization and disruption of intracellular targets. The presence of functional groups such as hydroxyl (-OH) and carboxylic acid (-COOH) moieties derived from HBAs facilitated close interaction between *Ft*-AgNPs and microbial cell membranes (Hernández-Díaz et al., 2021; Rodrigues et al., 2024). These interactions occurred through hydrogen bonding and electrostatic forces, collectively referred to as physical interactions. Upon approaching the cell surface, *Ft*-AgNPs physically disrupted the membrane structure, followed by internalization into the microbial cells.

The extent of internalization and antimicrobial performance was influenced by the physiochemical characteristics of the *Ft*-AgNPs. In this regard, parameters such as particle size, shape and degree of aggregation were critical (Menichetti et al., 2023). Smaller *Ft*-AgNPs can more readily penetrate microbial membranes, whereas larger or aggregated particles face restricted internalization. Given that the *Ft*-AgNPs synthesized in this study were predominantly spherical and had diameters below 10 nm as confirmed by SEM, TEM, an DLS analysis, their enhanced antimicrobial activity can be attributed to this favorable

10.3389/fnano.2025.1587084

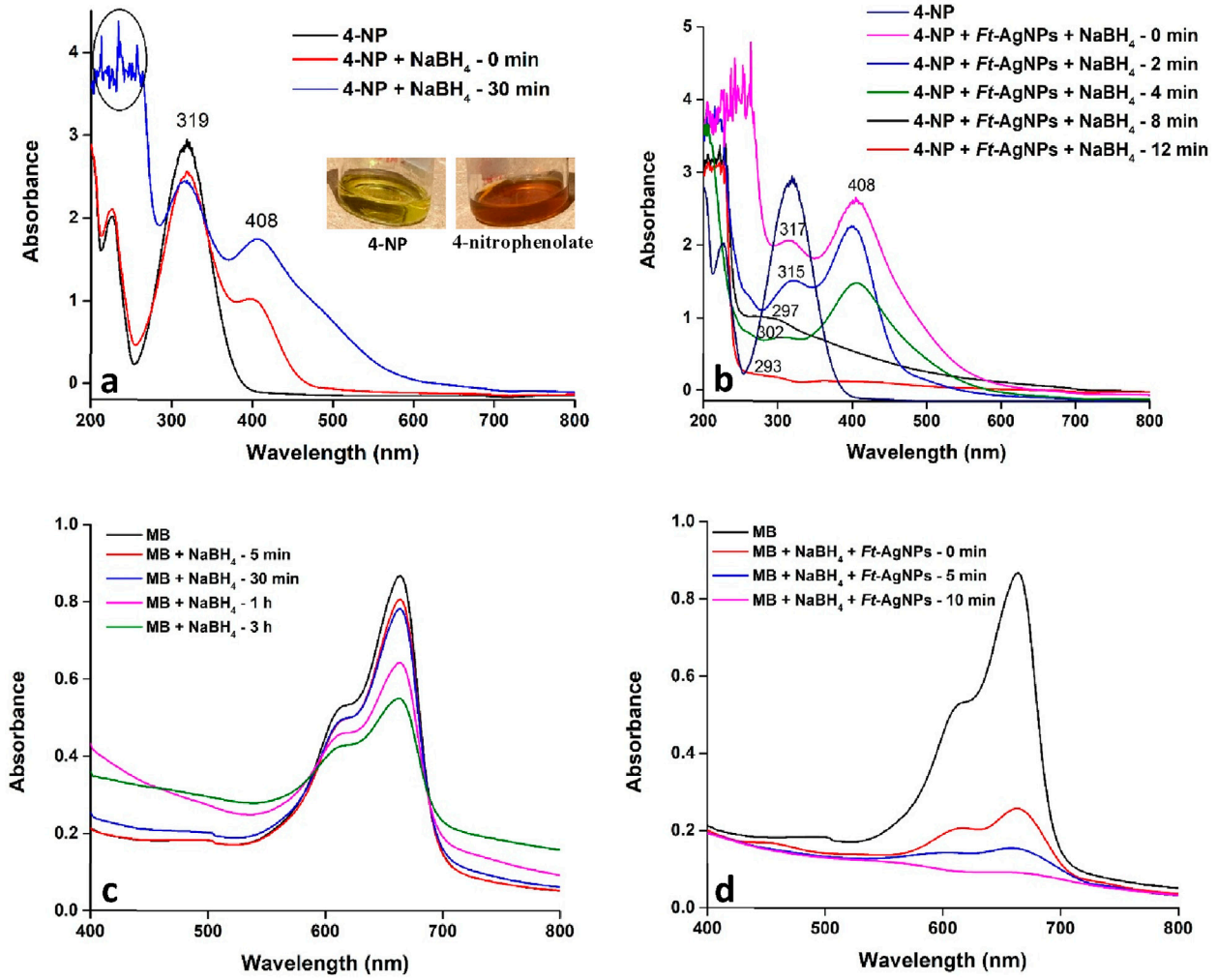

FIGURE 11
UV-Visible spectral analysis of the catalytic reduction of **(a)** 4-NP with $NaBH_4$, **(b)** 4-NP with *Ft*-AgNPs and $NaBH_4$, **(c)** MB with $NaBH_4$, and **(d)** MB with *Ft*-AgNPs and $NaBH_4$.

morphology and nanoscale size. The spherical shape, resulting from isotropic geometry, allowing uniform and close contact with microbial surfaces which further promoted cellular uptake. One internalized, *Ft*-AgNPs inflicted substantial intracellular damage by interacting with DNA, inducing the generation of ROS, releasing free radicals, and triggering electrolyte leakage. Additional damage was caused by the release of Ag^+ ions. These combined effects ultimately lead to microbial cell death. The proposed mechanism of action is illustrated in Scheme 3.

3.13 *Ft*-AgNPs as potential antioxidant agent

The antioxidant potential of *Ft*-AgNPs was evaluated using the DPPH (2,2-diphenyl-1-picrylhydrazyl) radical scavenging assay, a convenient visually indicative method for assessing antioxidant activity (Thomas and Thalla, 2023; Gulcin and Alwasel, 2023). In this assay, the characteristics purple color of the DPPH solution fades to colorless upon interaction with an antioxidant capable of neutralizing free radicals. Ascorbic acid (AA) was used as a standard reference. A fixed concentration of DPPH (50 μg/mL) was treated with increasing concentrations of *Ft*-AgNPs and AA. The resulting radical scavenging activities (%) were plotted against the respective concentrations, as shown in Figure 10a. *Ft*-AgNPs exhibited a concentration-dependent increase in DPPH scavenging activity, reaching approximately 84% at 50 μg/mL, while AA achieved a higher scavenging rate of about 95%–97% at the same concentration.

The significant antioxidant activity of *Ft*-AgNPs can be attributed to multiple mechanisms. Firstly, the surface functional groups (e.g., hydroxyl and carboxyl groups) present on *Ft*-AgNPs are capable of donating hydrogen radicals to stabilize the DPPH radicals. Secondly, *Ft*-AgNPs may also act as electron donors, undergoing oxidation and reducing DPPH to its non-radical (diamagnetic) form, as illustrated in the inset of Figure. Furthermore, the IC50 value, defined as the concentration required to scavenge 50% of DPPH radicals, was determined for both *Ft*-AgNPs and AA by plotting scavenging activity (%) against concentration (Figure 10b) using linear regression analysis. The IC_{50}, which indicate the antioxidant potency of each sample, was found to be 24.19 μg/mL for *Ft*-AgNPs and 23 μg/mL for AA,

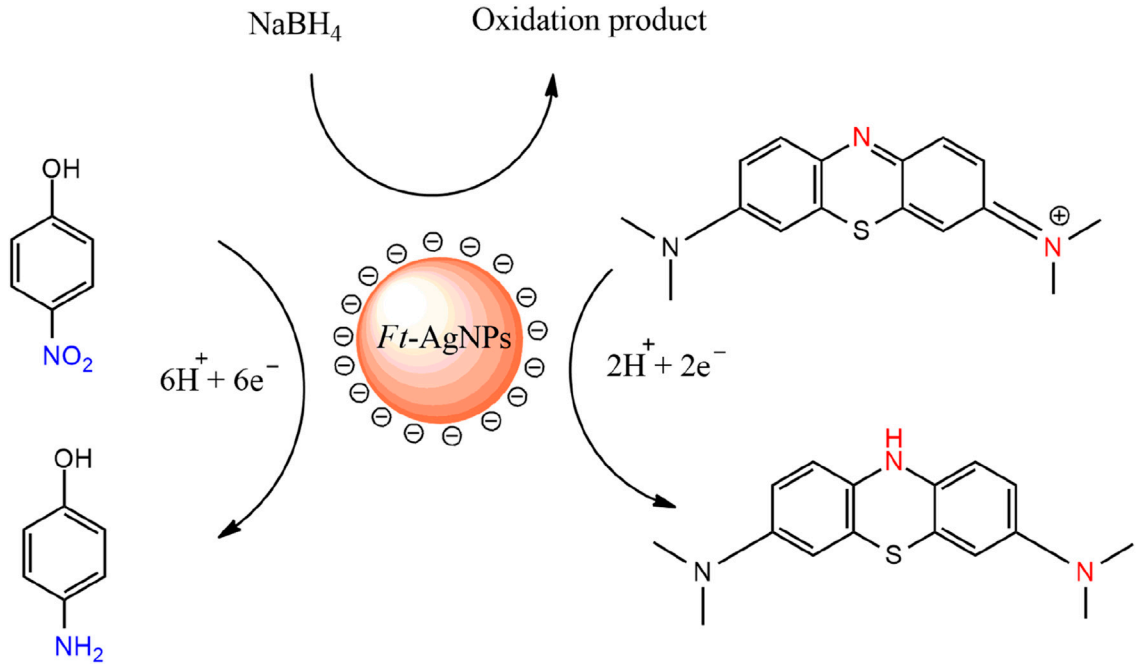

SCHEME 4
Simplified mechanism for the catalytic reduction of 4-NP and MB on the surface of *Ft*-AgNPs.

demonstrating that *Ft*-AgNPs exhibit comparable antioxidant activity to the standard.

3.14 Catalytic reduction efficiency of *Ft*-AgNPs

The catalytic efficiency of *Ft*-AgNPs for the reduction of 4-NP and MB in the presence of $NaBH_4$ was systematically assessed (Fatiqin et al., 2024; Charti et al., 2021). For this purpose, fixed concentrations of 4-NP and MB were separately mixed with an appropriate amount of *Ft*-AgNPs, and the reaction progress was monitored at regular intervals. The catalytic activity was tracked using UV-Visible spectroscopy across a wavelength range of 200–800 nm.

The 4-NP solution initially appeared yellow, which changed to dark brown upon the addition of $NaBH_4$ due to the formation of the 4-nitrophenolate ion. However, the solution did not decolorize completely, indicating that $NaBH_4$ alone was insufficient to fully reduce 4-NP to 4-aminophenol (4-AP). As shown in Figure 11a, the UV-Visible spectrum of 4-NP displayed an absorption peak at 319 nm, which slightly decreased after adding $NaBH_4$, while a new peak emerged at 408 nm, corresponding to the formation of 4-nitrophenolate ion. Figure 11b presents the UV-Visible spectra of 4-NP treated with both $NaBH_4$ and *Ft*-AgNPs. The data show a gradual decrease in the 319 nm peak and a corresponding increase in the 408 nm peak. Over time, in the presence of *Ft*-AgNPs, the 4-nitrophenolate ion was effectively reduced to 4-AP, marked by the appearance of a new peak at 297 nm, which eventually blue-shifted further. Complete conversion of 4-NP to 4-AP occurred within 12 min, a relatively short reaction time compared to previously reported studies (Edayadulla and Sundari, 2024; Shah et al., 2013), demonstrating the high catalytic efficiency of *Ft*-AgNPs.

The catalytic activity of *Ft*-AgNPs was further evaluated for the reduction of MB, a widely used fluorescent dye in the textile and food industries (Desai and Senta, 2015). Figures 11c,d present the UV-Visible spectra of MB treated with $NaBH_4$ at various time intervals. The characteristic absorption peak observed corresponds to the n-π^* transition of MB, consistent with previous reports (Liu et al., 2018). In the absence of *Ft*-AgNPs, the reduction of MB proceeded very slowly, with only a gradual decrease in absorption intensity and no complete decolorization even after 3 h. In contrast, the presence of *Ft*-AgNPs significantly enhanced the reduction rate, leading to complete decolorization within just 10 min. This marked improvement confirms the effective catalytic role of *Ft*-AgNPs in the reduction process.

The catalytic reduction mechanism can be explained as follows, $NaBH_4$ acts as the reducing agent, while 4-NP functions as the electrophilic substrate. *Ft*-AgNPs facilitate the reaction by providing an active surface that promotes rapid electron transfer from $NaBH_4$ to 4-NP, thereby accelerating the reduction process (Das and Das, 2022). A similar mechanism is observed in the case of MB, where MB is reduced to its lecu form on the surface of *Ft*-AgNPs, in agreement with previously reported pathways (Bhatu et al., 2024). A simplified representation of both mechanisms is illustrated in Scheme 4.

4 Conclusion

The green synthesis of *Ft*-AgNPs was effectively accomplished using the aqueous leaf extract of *F. tenacissima*. UV-visible, FTIR

and HPLC analysis confirmed the presence of HBAs in the extract, which served as both reducing agents for the conversion of Ag^{+} ions into *Ft*-AgNPs and as capping agents for their subsequent stabilization. SEM analysis revealed that *Ft*-AgNPs possessed a well-defined spherical morphology without noticeable aggregation, while TEM an DLS measurements confirmed their average size to be approximately 10 nm. The oxidized HBAs adsorbed onto the surface of the *Ft*-AgNPs played a key role in directing the nanoparticles toward microbial cells via hydrogen bonding and electrostatic interactions, thereby enhancing their antimicrobial activity. Furthermore, the small size and spherical shape of the *Ft*-AgNPs enabled them to penetrate and disrupt microbial cell membranes, ultimately leading to microbial death. Consequently, the *Ft*-AgNPs exhibited significant antimicrobial efficacy against *B. cereus*, *E. coli*, *P. aeruginosa*, *C. albicans*, and *C. glabrata* within the concentration range of 10–50 μg/mL. Notably, strong MIC and MBC values against *B. cereus* and *E. coli*, along with prolonged microbial susceptibility, suggest that *Ft*-AgNPs represent a promising alternative antimicrobial agent for infection treatment. In addition, their antioxidant activity, which was comparable to that of ascorbic acid, and their catalytic ability to efficiently reduce 4-NP and MB, further underscore their potential for applications in managing oxidative stress related diseases and in the removal of toxic pollutants from wastewater.

Despite the promising potential of *Ft*-AgNPs, several limitations should be acknowledged. First, antimicrobial testing was conducted against a limited number of microbial strains due to their unavailability. Testing across a broader range of resistant or clinically relevant pathogens would strengthen the study's conclusions. Second, the synthesis of *Ft*-AgNPs and their observed antimicrobial, antioxidant, and catalytic activities rely heavily on on the phytochemical present in the aqueous extract *F. tenacissima*. However, variations in plant growth conditions, harvesting timing, and extraction protocols may affect the reproducibility and consistency of the *Ft*-AgNPs and their associated properties. Additionally, the proposed antimicrobial mechanism is primarily from existing literature and general trends, rather than being confirmed through direct experimental validation. Incorporating mechanistic studies would further substantiate these claims. Lastly, although the cytotoxicity of *Ft*-AgNPs is expected to be low due to surface passivation and favourable physicochemical characteristics, more comprehensive evaluations are necessary, Specifically, *in vitro* cytotoxicity assays, including MTT, LDH release, and ROS generation studies using human cell lines, are essential to validate the predicted minimal cytotoxicity and high biocompatibility of *Ft*-AgNPs for safe biomedical applications. These aspects will be a key focus in our future investigations.

Data availability statement

The original contributions presented in the study are included in the article/supplementary material, further inquiries can be directed to the corresponding authors.

Author contributions

HSA: Conceptualization, Data curation, Formal Analysis, Investigation, Methodology, Writing – original draft, Writing – review and editing. MSA: Data curation, Methodology, Writing – review and editing. NB: Conceptualization, Data curation, Investigation, Methodology, Writing – original draft, Writing – review and editing. HIA: Data curation, Formal Analysis, Investigation, Methodology, Writing – review and editing. NA: Data curation, Formal Analysis, Investigation, Methodology, Writing – original draft, Writing – review and editing. MA: Investigation, Methodology, Formal analysis, Writing – original draft, Writing – review and editing. SC: Investigation, Methodology, Formal analysis, Writing – original draft, Writing – review and editing. MS: Conceptualization, Data curation, Formal Analysis, Investigation, Methodology, Writing – original draft, Writing – review and editing. AK: Conceptualization, Data curation, Formal Analysis, Investigation, Methodology, Writing – original draft, Writing – review and editing.

Funding

The author(s) declare that no financial support was received for the research and/or publication of this article.

Acknowledgments

The authors wish to thank the Chemistry Department, Faculty of Science, King Abdulaziz University, the Center of Excellence in Environmental Studies, and the Ministry of Higher Education (MoHE), KSA, for their support during this work.

Conflict of interest

The authors declare that the research was conducted in the absence of any commercial or financial relationships that could be construed as a potential conflict of interest.

Generative AI statement

The author(s) declare that no Generative AI was used in the creation of this manuscript.

Publisher's note

All claims expressed in this article are solely those of the authors and do not necessarily represent those of their affiliated organizations, or those of the publisher, the editors and the reviewers. Any product that may be evaluated in this article, or claim that may be made by its manufacturer, is not guaranteed or endorsed by the publisher.

References

Alfei, S., Caviglia, D., Penco, S., Zuccari, G., and Gosetti, F. (2022). 4-Hydroxybenzoic acid as an antiviral product from alkaline autoxidation of catechinic acid: a fact to be reviewed. *Plants* 11, 1822. doi:10.3390/plants11141822

Alharbi, N. S., Alsubhi, N. S., and Felimban, A. I. (2022). Green synthesis of silver nanoparticles using medicinal plants: characterization and application. *J. Radiat. Res. Appl. Sci.* 15, 109–124. doi:10.1016/j.jrras.2022.06.012

Aljamali, N. M., Al-zubaidy, Z. H., and Enad, A. H. (2021). Bacterial infection and common bacterial diseases: a review. *Pharm. Nanotechnol.* 3, 13–23.

Anand, U., Carpena, M., Kowalska-Góralska, M., Garcia-Perez, P., Sunita, K., Bontempi, E., et al. (2022). Safer plant-based nanoparticles for combating antibiotic resistance in bacteria: a comprehensive review on its potential applications, recent advances, and future perspective. *Sci. Total Environ.* 821, 153472. doi:10.1016/j.scitotenv.2022.153472

Andreani, A. S., Kunarti, E. S., and Santosa, S. J. (2019). Synthesis of gold nanoparticles capped-benzoic acid derivative compounds (o-m-and p-hydroxybenzoic acid). *Indonesian J. Chem.* 19, 376–385. doi:10.22146/ijc.34440

Assaf, H. K., Nafady, A. M., Abdelkader, M. S., Allam, A. E., and Kamel, M. S. (2015). Phytochemical and biological studies of aerial parts of *Forsskaolea tenacissima* linn. (urticaceae). *J. Pharmacogn. Phytochemistry* 4, 282–287.

Assaf, H. K., Nafady, A. M., Allam, A. E., Hamed, A. N. E., Kamel, M. S., and Shimizu, K. (2018). Forsskamide, a new ceramide from aerial parts of *Forsskaolea tenacissima* linn. *Nat. Prod. Res.* 32, 2452–2456. doi:10.1080/14786419.2017.1419234

Assaf, H. K., Nafady, A. M., Allam, A. E., Hamed, A., and Kamel, M. S. (2021). Phytochemistry and biological activity of family urticaceae: a review (1957–2019). *SSRN Electron. J.* doi:10.2139/ssrn.3776660

Azad, A., Zafar, H., Raza, F., and Sulaiman, M. (2023). Factors influencing the green synthesis of metallic nanoparticles using plant extracts: a comprehensive review. *Pharm. Fronts* 5, e117–e131. doi:10.1055/s-0043-1774289

Bashami, R. M., Soomro, M. T., Khan, A. N., Aazam, E. S., Ismail, I. M. I., and El-Shahawi, M. S. (2018). A highly conductive thin film composite based on silver nanoparticles and malic acid for selective electrochemical sensing of trichloroacetic acid. *Anal. Chim. Acta* 1036, 33–48. doi:10.1016/j.aca.2018.06.084

Bérdy, J. (2012). Thoughts and facts about antibiotics: where we are now and where we are heading. *J. Antibiotics* 65, 385–395. doi:10.1038/ja.2012.27

Bhatu, M. N., Mavlankar, G. R., Baviskar, R., Patil, A. B., and Patil, S. P. (2024). Ag-based bimetallic nanoparticles for the catalytic reduction of nitrophenol and organic dyes: an overview. *ChemistrySelect* 9, e202304200. doi:10.1002/slct.202304200

Charti, I., Azouzi, A., Belghiti, A., Sair, S., Abboud, Y., and El Bouari, A. (2021). Ecofriendly synthesis of stabilized silver nanoparticles and the evaluation of their potential applications. *Curr. Res. Green Sustain. Chem.* 4, 100102. doi:10.1016/j.crgsc.2021.100102

Cohen, M. A., Huband, M. D., Mailloux, G. B., Yoder, S. L., Roland, G. E., Domagala, J. M., et al. (1991). *In vitro* antibacterial activities of PD 131628, a new 1,8-naphthyridine anti-infective agent. *Antimicrob. Agents Chemother.* 35, 141–146. doi:10.1128/aac.35.1.141

Das, T. K., and Das, N. C. (2022). Advances on catalytic reduction of 4-nitrophenol by nanostructured materials as benchmark reaction. *Int. Nano Lett.* 12, 223–242. doi:10.1007/s40089-021-00362-w

Desai, N. C., and Senta, R. D. (2015). Simultaneous Rp-HPLC determination of salicylamide, salicylic acid and deferasirox in the bulk API dosages forms. *J. Taibah Univ. Sci.* 9, 245–251. doi:10.1016/j.jtusci.2014.11.006

Edayadulla, N., and Sundari, C. S. S. (2024). "Role of stabilizing agent role in nanomaterials (NM)," in *Sustainable green synthesised nano-dimensional materials for energy and environmental applications* (Boca Raton, FL: CRC Press), 47–63. doi:10.1201/9781003362241

Fatiqin, A., Alfanaar, R., Rahman, S., Febrianto, Y., Citrariana, S., Arsana, M. P., et al. (2024). Catalytic reduction of 4-nitrophenol and methylene blue with silver nanoparticles decorated with *drymoglossum Piloselloides* extract. *J. Multidiscip. Appl. Nat. Sci.* 4, 249–261. doi:10.47352/jmans.2774-3047.210

Feofilova, E. P. (2010). The fungal cell wall: modern concepts of its composition and biological function. *Microbiology* 79, 711–720. doi:10.1134/S0026261710060019

Frère, J.-M., and Rigali, S. (2016). The alarming increase in antibiotic-resistant bacteria. *Drug Target Rev.* 3, 26–30.

Gonzalez-Fuenzalida, R. A., Moliner-Martinez, Y., Molins-Legua, C., Parada-Artigues, V., Verdu-Andres, J., and Campins-Falco, P. (2016). New tools for characterizing metallic nanoparticles: agnps, a case study. *Anal. Chem.* 88, 1485–1493. doi:10.1021/acs.analchem.5b04751

Gulcin, İ., and Alwasel, S. H. (2023). DPPH radical scavenging assay. *Processes* 11, 2248. doi:10.3390/pr11082248

Hernández-Díaz, J. A., Garza-García, J. J. O., Zamudio-Ojeda, A., León-Morales, J. M., López-Velázquez, J. C., and García-Morales, S. (2021). Plant-mediated synthesis of nanoparticles and their antimicrobial activity against phytopathogens. *J. Sci. Food Agric.* 101, 1270–1287. doi:10.1002/jsfa.10767

Jahani, S., Saeidi, S., Javadian, F., Akbarizadeh, Z., and Sobhanizade, A. (2016). Investigating the antibacterial effects of plant extracts on *Pseudomonas aeruginosa* and *Escherichia coli*. *Int. J. Infect.* 3, e34081. doi:10.17795/iji-34081

Kaabipour, S., and Hemmati, S. (2021). A review on the green and sustainable synthesis of silver nanoparticles and one-dimensional silver nanostructures. *Beilstein J. Nanotechnol.* 12, 102–136. doi:10.3762/bjnano.12.9

Katsipoulaki, M., Stappers, M. H., Malavia-Jones, D., Brunke, S., Hube, B., and Gow, N. A. (2024). Candida albicans and candida glabrata: global priority pathogens. *Microbiol. Mol. Biol. Rev.* 88, e00021–23. doi:10.1128/mmbr.00021-23

Katzenberger, R. H., Rösel, A., and Vonberg, R.-P. (2021). Bacterial survival on inanimate surfaces: a field study. *BMC Res. Notes* 14, 97. doi:10.1186/s13104-021-05492-0

Kaur, N. (2024). An innovative outlook on utilization of agro waste in fabrication of functional nanoparticles for industrial and biological applications: a review. *Talanta* 267, 125114. doi:10.1016/j.talanta.2023.125114

Khan, A. N., Aldowairy, N. N. A., Alorfi, H. S. S., Aslam, M., Bawazir, W. A., Hameed, A., et al. (2022). Excellent antimicrobial, antioxidant, and catalytic activities of medicinal plant aqueous leaf extract derived silver nanoparticles. *Processes* 10, 1949. doi:10.3390/pr10101949

Kirthika, V., Gunasekar, B., Pal, D. B., Kumar, S., and Kapoor, A. (2025). Biogenic synthesis of silver nanoparticles using Parthenium hysterophorus floral extract and their multifaceted biomedical applications. *Plant Nano Biol.* 12, 100148. doi:10.1016/j.plana.2025.100148

Kulkarni, A. G., De Britto, S., and Jogaiah, S. (2021). "Economic considerations and limitations of green synthesis vs chemical synthesis of nanomaterials," in *Advances in nano-fertilizers and nano-pesticides in agriculture* (Woodhead Publishing), 459–468. doi:10.1016/B978-0-12-820092-6.00018-5

Liu, Y.-S., Chang, Y.-C., and Chen, H.-H. (2018). Silver nanoparticle biosynthesis by using phenolic acids in rice husk extract as reducing agents and dispersants. *J. Food Drug Analysis* 26, 649–656. doi:10.1016/j.jfda.2017.07.005

Mansur, S. M., and Yahya, R. T. (2025). Green synthesis of silver nanoparticles Ag-NPs using tomato (*Solanum lycopersicum*) fruit extract and detection them. *Egypt. J. Veterinary Sci.*, 1–10. doi:10.21608/ejvs.2024.290217.2099

Martemucci, G., Costagliola, C., Mariano, M., D'Andrea, L., Napolitano, P., and D'Alessandro, A. G. (2022). Free radical properties, source and targets, antioxidant consumption and health. *Oxygen* 2, 48–78. doi:10.3390/oxygen2020006

Mateo, E. M., and Jiménez, M. (2022). Silver nanoparticle-based therapy: can it be useful to combat multi-drug resistant bacteria? *Antibiotics* 11, 1205. doi:10.3390/antibiotics11091205

Menichetti, A., Mavridi-Printezi, A., Mordini, D., and Montalti, M. (2023). Effect of size, shape and surface functionalization on the antibacterial activity of silver nanoparticles. *J. Funct. Biomaterials* 14, 244. doi:10.3390/jfb14050244

Moloney, M. G. (2016). Natural products as a source for novel antibiotics. *Trends Pharmacol. Sci.* 37, 689–701. doi:10.1016/j.tips.2016.05.001

More, P. R., Pandit, S., De Filippis, A., Franci, G., Mijakovic, I., and Galdiero, M. (2023). Silver nanoparticles: bactericidal and mechanistic approach against drug resistant pathogens. *Microorganisms* 11, 369. doi:10.3390/microorganisms11020369

Mughal, T. A., Ali, S., Mumtaz, S., Summer, M., Saleem, M. Z., Hassan, A., et al. (2024). Evaluating the biological (antidiabetic) potential of TEM, FTIR, XRD, and UV-spectra observed *berberis Lyceum* conjugated silver nanoparticles. *Microsc. Res. Tech.* 87, 1286–1305. doi:10.1002/jemt.24509

Nurkhaliza, F., Risana, M. Z., Pubasari, A., Priatmoko, S., Prastya, M. E., and Andreani, A. S. (2024). "Comparative study of well diffusion and disc diffusion method to investigate the antibacterial properties of silver nanoparticles synthesized from *Curcuma longa* extracts,"*E3S Web Conf*, 503. doi:10.1051/e3sconf/202450309003

Nie, P., Zhao, Y., and Xu, H. (2023). Synthesis, applications, toxicity and toxicity mechanisms of silver nanoparticles: a review. *Ecotoxicol. Environ. Saf.* 253, 114636. doi:10.1016/j.ecoenv.2023.114636

Nwabor, O. F., Singh, S., Wunnoo, S., Lerwittayanon, K., and Voravuthikunchai, S. P. (2021). Facile deposition of biogenic silver nanoparticles on porous alumina discs, an efficient antimicrobial, antibiofilm, and antifouling strategy for functional contact surfaces. *Biofouling* 37, 538–554. doi:10.1080/08927014.2021.1934457

Nwobodo, D. C., Ugwu, M. C., Anie, C. O., Al-Ouqaili, M. T. S., Ikem, J. C., Chigozie, U. V., et al. (2022). Antibiotic resistance: the challenges and some emerging strategies for tackling a global menace. *J. Clin. Laboratory Analysis* 36, e24655. doi:10.1002/jcla.24655

Palithya, S., Gaddam, S. A., Kotakadi, V. S., Penchalaneni, J., and Challagundla, V. N. (2021). Biosynthesis of silver nanoparticles using leaf extract of *Decaschistia crotonifolia* and its antibacterial, antioxidant, and catalytic applications. *Green Chem. Lett. Rev.* 14, 137–152. doi:10.1080/17518253.2021.1876172

Paseban, N., Ghadam, P., and Pourhosseini, P. S. (2019). The fluorescence behavior and stability of AgNPs synthesized by *Juglans regia* green husk aqueous extract. *Int. J. Nanosci. Nanotechnol.* 15, 117–126.

Patel, R. R., Singh, S. K., and Singh, M. (2023). Green synthesis of silver nanoparticles: methods, biological applications, delivery and toxicity. *Mater. Adv.* 4, 1831–1849. doi:10.1039/d2ma01105k

Rodrigues, A. S., Batista, J. G. S., Rodrigues, M. Á. V., Thipe, V. C., Minarini, L. A. R., Lopes, P. S., et al. (2024). Advances in silver nanoparticles: a comprehensive review on their potential as antimicrobial agents and their mechanisms of action elucidated by proteomics. *Front. Microbiol.* 15, 1440065. doi:10.3389/fmicb.2024.1440065

Roy, P., Das, B., Mohanty, A., and Mohapatra, S. (2017). Green synthesis of silver nanoparticles using Azadirachta indica leaf extract and its antimicrobial study. *Appl. Nanosci.* 7, 843–850. doi:10.1007/s13204-017-0621-8

Sadiq, I. Z. (2023). Free radicals and oxidative stress: signaling mechanisms, redox basis for human diseases, and cell cycle regulation. *Curr. Mol. Med.* 23, 13–35. doi:10.2174/1566524022666211222161637

Sánchez, G. R., Lagos Castilla, C., Benito Gómez, N., García, A., Marcos, R., and Carmona, E. R. (2016). Leaf extract from the endemic plant *Peumus boldus* as an effective bioproduct for the green synthesis of silver nanoparticles. *Mater. Lett.* 183, 255–260. doi:10.1016/j.matlet.2016.07.115

Shah, S., Dhanani, T., and Kumar, S. (2013). Validated HPLC method for identification and quantification of p-hydroxy benzoic acid and agnuside in *Vitex negundo* and *Vitex trifolia*. *J. Pharm. Analysis* 3, 500–508. doi:10.1016/j.jpha.2013.09.008

Sher, A., Afzal, M., and Bakht, J. (2017). Pharmacological evaluation of different extracts of *Forsskaolea tenacissima*. *Indian J. Pharm. Sci.* 79, 208–213. doi:10.4172/pharmaceutical-sciences.1000224

Sieuwerts, S., De Bok, F. A. M., Mols, E., De Vos, W. M., and van Hylckama Vlieg, J. E. T. (2008). A simple and fast method for determining colony forming units. *Lett. Appl. Microbiol.* 47, 275–278. doi:10.1111/j.1472-765x.2008.02417.x

Singhal, G., Bhavesh, R., Kasariya, K., Sharma, A. R., and Singh, R. P. (2011). Biosynthesis of silver nanoparticles using Ocimum sanctum (tulsi) leaf extract and screening its antimicrobial activity. *J. nanoparticle Res.* 13, 2981–2988. doi:10.1007/s11051-010-0193-y

Smith, R. P., Baltch, A. L., Hammer, M. C., and Conroy, J. V. (1988). *In vitro* activities of PD 117,596 and reference antibiotics against 448 clinical bacterial strains. *Antimicrob. Agents Chemother.* 32, 1450–1455. doi:10.1128/aac.32.9.1450

Subramani, K., Wutthithien, P., Saha, R., Lindblad, P., and Incharoensakdi, A. (2024). Characterization and potentiality of plant-derived silver nanoparticles for enhancement of biomass and hydrogen production in chlorella sp. under nitrogen deprived condition. *Chemosphere* 361, 142514. doi:10.1016/j.chemosphere.2024.142514

Sun, Y., Zhou, L., Liao, T., Liu, J., Yu, K., Zou, L., et al. (2022). Comparing the effect of benzoic acid and cinnamic acid hydroxyl derivatives on polyphenol oxidase: activity, action mechanism, and molecular docking. *J. Sci. Food Agric.* 102, 3771–3780. doi:10.1002/jsfa.11725

Thanh, N. C., Pugazhendhi, A., Chinnathambi, A., Alharbi, S. A., Subramani, B., Brindhadevi, K., et al. (2022). Silver nanoparticles (AgNPs) fabricating potential of aqueous shoot extract of *Aristolochia bracteolata* and assessed their antioxidant efficiency. *Environ. Res.* 208, 112683. doi:10.1016/j.envres.2022.112683

Thomas, T., and Thalla, A. K. (2023). Synthesis of silver nanoparticles using *Myristica fragrans* seed shell: assessment of antibacterial, antioxidant properties and photocatalytic degradation of dyes. *J. Environ. Chem. Eng.* 11, 109585. doi:10.1016/j.jece.2023.109585

Tripathi, N., and Goshisht, M. K. (2022). Recent advances and mechanistic insights into antibacterial activity, antibiofilm activity, and cytotoxicity of silver nanoparticles. *ACS Appl. Bio Mater.* 5, 1391–1463. doi:10.1021/acsabm.2c00014

Uyttebroek, S., Chen, B., Onsea, J., Ruythooren, F., Debaveye, Y., Devolder, D., et al. (2022). Safety and efficacy of phage therapy in difficult-to-treat infections: a systematic review. *Lancet Infect. Dis.* 22, e208–e220. doi:10.1016/s1473-3099(21)00612-5